Nuclear Physics B302 (1988) 1–64
North-Holland, Amsterdam

A NON-PERTURBATIVE ANALYSIS IN FINITE VOLUME GAUGE THEORY

Jeffrey KOLLER[1] and Pierre van BAAL[2]

Institute for Theoretical Physics, State University of New York at Stony Brook, Stony Brook, New York 11794-3840, USA

Received 25 August 1987

We discuss SU(2) gauge theory on a three-torus using a finite volume expansion. Our discovery of natural coordinates allows us to obtain continuum results in a region where Monte Carlo data are also available. The obtained results agree well with the perturbative and semiclassical analysis for small volumes, and there is fair agreement with the Monte Carlo results in intermediate volumes. The simple picture which emerges for the approximate low energy dynamics is that of three interacting particles enclosed in a sphere, with zero total "angular momentum". The validity of an adiabatic approximation is investigated. The fundamentally new understanding gained, is that non-perturbative dynamics can be incorporated by imposing boundary conditions which arise through the nontrivial topology of configuration space.

1. Introduction

The subject of non-perturbative effects in gauge theories is a difficult one from an analytic point of view, and has been approached from many directions. There has been only limited success, and the main prize, the understanding and a reasonably rigorous proof of confinement, is still unclaimed. In previous work, we advocated first understanding QCD in a small volume, then working outwards to larger volumes, to the scale where confinement effects begin. The foundations for such an approach were laid in 't Hooft's study [1] of gauge theories on a torus, and the small scale perturbative domain was analysed by Lüscher in his contribution [3]. In our semiclassical work [4], we identified the point where non-perturbative behaviour first breaks out, but showed it could not be the onset of confinement. We gave circumstantial evidence for a second outbreak, at even larger volumes, which *is* associated with string formation and confinement. In keeping with our philosophy, we set ourselves the task of understanding the first type of non-perturbative behaviour, to prepare a firm base for an eventual assault on the confining domain.

This paper analyses the dynamics of SU(2) QCD in the intermediate regime, between the perturbative domain and the string domain. A letter describing some of

Present addresses:
[1] Lauritsen Lab., Mailcode 352-48, CALTECH, Pasadena, CA 91125, USA.
[2] CERN, Theory Division, CH-1211 Geneva 23, Switzerland.

our results has already been published [6], so we concentrate here on our methods and the insights obtained into non-perturbative behaviour.

We work [4] in the hamiltonian formalism, on a symmetric three-torus of length L. A low-energy effective hamiltonian for this problem was derived by Lüscher by perturbatively integrating out all modes except the spatially constant (zero momentum) ones. Lüscher and Münster then solved this effective hamiltonian using perturbation theory, properly taking into account the quartic nature of these modes [3]. The perturbative expansion is equivalent to a small volume expansion, since one renormalises using minimal subtraction at the scale L. The essence of our approach is noting that Lüscher's effective hamiltonian is accurate even at distance scales where it cannot be solved perturbatively. Thus, it is still valid to derive it perturbatively, even though it is not valid to solve it perturbatively. We consider our results accurate up to $L \sim 5M(0^+)^{-1}$, where $M(0^+)$ is the scalar glueball mass (~ 1 GeV), whereas the perturbative solutions are (in general) demonstrably inaccurate beyond $1M(0^+)^{-1}$. Perturbation theory breaks down here not because the expansion parameter is large, but because topological properties of configuration space become important.

To properly account for the topology of configuration space, one must understand the vacuum valley $\mathscr{V}$, which is the set of gauge-inequivalent classical vacua of the Yang-Mills hamiltonian:

$$\mathscr{V} = \mathscr{N}/\mathscr{G}. \tag{1.1}$$

Here $\mathscr{N}$ is the null set of the Yang Mills potential

$$\mathscr{N} = \left\{ A_i(x) \middle| A_i(x+L) = A_i(x),\ \int_{T_3} \mathrm{d}^3x\, \mathrm{Tr}\big(F_{ij}^2(x)\big) = 0 \right\}, \tag{1.2}$$

and $\mathscr{G}$ is the set of local gauge transformations

$${}^g A_i(x) = g(x) A_i(x) g(x)^{-1} - ig(x)\, \partial_i g(x)^{-1}. \tag{1.3}$$

As usual, $A_i(x)$ is here the Lie algebra-valued vector potential

$$A_i(x) = A_i^a(x) \frac{\sigma_a}{2}, \tag{1.4}$$

and $F_{ij}(x)$ is the chromomagnetic field strength

$$F_{ij}(x) = \partial_i A_j(x) - \partial_j A_i(x) + i\big[A_i(x), A_j(x)\big], \tag{1.5}$$

written similarly in terms of the Pauli matrices σ_i. Finally, $g(x)$ is an SU(2)-valued

function on the three torus:

$$g(\boldsymbol{x}+L\boldsymbol{e}_i)=g(\boldsymbol{x})\,. \tag{1.6}$$

We showed in ref. [4] that $\mathscr{V}$ is the disconnected union of spaces $\mathscr{V}_P$ with distinct integer topological quantum number P. The gauge transformation eq. (1.3) maps $\mathscr{V}_0$ into $\mathscr{V}_P$ if $g(x)$ has Pontryagin index P:

$$P=\frac{1}{24\pi^2}\int_{\mathrm{T}^3}\mathrm{d}^3x\,\varepsilon_{ijk}\mathrm{Tr}\big(\big(g\,\partial_i g^{-1}\big)\big(g\,\partial_j g^{-1}\big)\big(g\,\partial_k g^{-1}\big)\big)\,, \tag{1.7}$$

and each $\mathscr{V}_P$ is a three-torus with periods 4π:

$$\mathscr{V}_0=\left\{\boldsymbol{C}\in(R/4\pi Z)^3\right\}. \tag{1.8}$$

Actually, to be accurate, it is an "orbifold", $\mathrm{T}^3/\mathrm{Z}_2^3$, but our arguments will account for this implicitly. From now on, we work in a single sector, $\mathscr{V}_0$, and drop the subscript.

The electric flux quantum number is introduced by recognising that the theory has additional symmetries, the so-called "allowed gauge transformations", which are antiperiodic SU(2)-valued functions,

$$g(\boldsymbol{x}+L\boldsymbol{e}_i)=(-1)^{k_i}g(x)\,, \tag{1.9}$$

acting by the normal gauge transformation formula (1.3). Here $\boldsymbol{k}$ is the Z_2-valued 't Hooft twist vector. These are not gauge symmetries, because states are allowed to transform nontrivially under them:

$$|\Psi({}^{g}A(x))\rangle=(-1)^{\boldsymbol{k}\cdot\boldsymbol{e}}|\Psi(A(x))\rangle\,, \tag{1.10}$$

where $\boldsymbol{e}$ is the Z_2-valued electric flux of $|\Psi(A(x))\rangle$.

We will show in sect. 3 that Lüscher's effective hamiltonian is equivalent to an infinite component hamiltonian on the vacuum valley. Moreover, in sect. 4 we will show that this wave function must vanish at $C_i=2\pi n_i$, $(\boldsymbol{n}\in(\mathrm{Z}_2)^3)$. Thus we arrive at an effective theory defined on the cube $[0,2\pi]^3$, with vanishing boundary conditions.

This is a satisfying result, because it explains neatly why the vacuum valley has the symmetry $(\mathrm{Z}_2)^3$ rather than the full group of translations on the torus. The $(\mathrm{Z}_2)^3$ arises from the allowed gauge transformations eq. (1.9) with non-trivial homotopy, which map the cube into itself. In particular, the eight corners of the cube correspond to eight equivalent perturbative quantum vacua, which can be mapped into each other by these transformations. Other points, within the vacuum

valley cube, are not quantum vacua because quantum effects raise the energy of the system in these configurations. This can be interpreted as a quantum-induced potential barrier separating the eight perturbative vacua.

It is now easy to see the origin of the non-perturbative effect we are discussing here, and the concept of electric flux energy. At small coupling, a perturbation expansion within any of the wells will give accurate results. There are thus eight degenerate perturbative vacua. However, as the coupling increases, the energies approach the barrier height, and the system tunnels from one vacuum to another. The eight degenerate levels split, the true non-perturbative vacuum being a symmetric linear combination of the eight perturbative vacuum states. The other seven linear combinations transform non-trivially under the allowed gauge transformations, eq. (1.9), and thus have nonzero electric flux. The energy split is the energy of electric flux. To avoid confusion, we should point out that even at very small values of the coupling there is *some* tunneling between the wells, giving an exponentially small energy of electric flux. However, we say "tunneling sets in" where the splitting of the levels becomes appreciable on the energy scale of the levels themselves. This is typically where the exponential in the semiclassical splitting formula becomes O(1).

In this paper we show how to approximately include in Lüscher's effective hamiltonian the effects of additional perturbative vacua. The idea is to introduce boundary conditions "midway between the wells", chosen to enforce the correct symmetry of the wave function, and then work in a single well.

In sect. 2 we describe a background field calculation to compute Lüscher's effective hamiltonian to higher orders. This calculation reveals a new coordinate system for the zero-momentum gauge fields, which allows the Rayleigh-Ritz calculation of low-lying energies. In sect. 3 we discuss writing the theory as an infinite component hamiltonian on the vacuum valley. Our earlier semiclassical work [4] used either gauge-fixed coordinates, which had Gribov ambiguities, or polar coordinates, which were messy in the nonspherical sector. Our new coordinates differ from the old ones in their parameterisation of degrees of freedom transverse to the vacuum valley. They are actually singular at certain points, but only in the way spherical coordinates are singular at the origin, and this singularity is what causes the wave function to vanish at the boundaries of $\mathscr{V}$. A different choice of transverse coordinates, with different or no singularities, can lead to a different decomposition along the vacuum valley, and some of the subtleties involved are discussed in sects. 3 and 7.

In sect. 4 we discuss configuration space boundary conditions as an effective way of incorporating the topological non-triviality. The intimate connection with Gribov ambiguities is discussed in detail. We show how this problem could be approached in general, and then argue boldly that if the adiabatic approximation is accurate on the boundary, the boundary conditions in our new coordinates are unique and elegant.

The new coordinates would be a bad choice for a semiclassical analysis, but do allow an elegant elimination of the gauge degrees of freedom in a Rayleigh-Ritz calculation. Sect. 5 finds the low-lying spectrum of the resulting theory using the Rayleigh-Ritz method. A numerical method is inevitable, since the hamiltonian is nonintegrable, but we take pains to calculate matrix elements analytically and to provide rigorous upper and lower bounds for the results.

We consider it crucial that our new results agree with our previous semiclassical results. This is shown in sect. 6. In sect. 7 we check that the adiabatic approximation is valid on the boundary, and conclude that it is, to within a few percent. Finally, in sect. 8, we address the consequences our results have for many issues of physics. We conclude with two technical appendices and an outline of our approach applied to a simple toy model.

2. The background field calculation

In this section we rederive the effective lagrangian for spatially constant gauge fields, using the non-local gauge fixing procedure suggested in ref. [8]. For details we refer the reader to [4].

The gauge field A_μ is split into a constant piece $B_\mu(t)$ and a spatially varying piece $Q_\mu(t, \boldsymbol{x})$:

$$B_\mu = \frac{1}{L^3}\int_{\mathrm{T}^3} \mathrm{d}^3x\, A_\mu(x) \equiv \mathscr{P} A_\mu . \tag{2.1}$$

The gauge fixing then sets $B_0 = 0$ in the B sector, and introduces a gauge fixing term and ghosts $\Psi, \overline{\Psi}$ in the Q sector. The quantum modes Q_μ are integrated out, leaving an effective action for B_i [4]:

$$\begin{aligned} iS_{\mathrm{eff}} &= i\int \mathrm{d}t\, \mathscr{L}_{\mathrm{eff}}(B) \\ &= \ln \int \mathscr{D}'Q_\mu \mathscr{D}'\Psi \mathscr{D}'\overline{\Psi} \exp\left[-\frac{i}{g_0^2}\int \mathrm{d}t \int_{\mathrm{T}^3} \mathrm{d}^3x\, \mathscr{L}(B, Q, \Psi, \overline{\Psi})\right], \end{aligned}$$

$$\begin{aligned} \mathscr{L}(B, Q, \Psi, \overline{\Psi}) = \mathrm{Tr}\Big\{ &\tfrac{1}{2}\big(F_{\mu\nu}(B+Q)\big)^2 - \big(D_\mu(B)Q_\mu\big)^2 - 2\overline{\Psi} D_\mu(B)\, D_\mu(B+Q)\Psi \\ &- 2\big[Q_\mu, \Psi\big]\mathscr{P}\big[Q_\mu, \overline{\Psi}\big]\Big\}. \end{aligned} \tag{2.2}$$

The primes in the integration remind us to omit zero momentum modes. Ref. [9] gives Feynman rules for this problem.

We will first compute the one-loop part of S_{eff} quadratic in B. The diagrams are shown in fig. 1. Momentum $p = (p_0, \mathbf{0})$ flows through the graph, i.e., external spatial

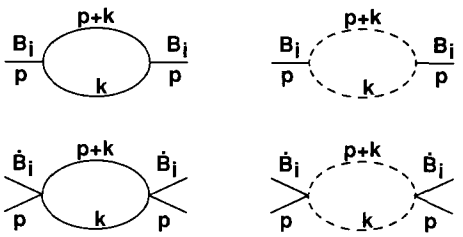

Fig. 1. Feynman diagrams for the one-loop effective action, quadratic in the background field B (eq. (2.3)). For the Feynman rules see ref. [9].

momenta are zero. We obtain

$$S_{\text{eff}}(\text{1-loop, fig. 1}) = -\int \mathrm{d}t\,\mathrm{d}t'\,\mathrm{d}p_0\,\mathrm{e}^{ip_0(t-t')}\frac{1}{2\pi}\,\mathrm{Tr}\big(B_i(t)B_j(t')\big) \times \sum_{Lk/2\pi\in Z^d} \frac{\frac{1}{2}(d-1)k_ik_j + p_0^2\delta_{ij}}{|k|\big(k^2+\frac{1}{4}p_0^2\big)}, \tag{2.3}$$

where $d = 3 - 2\varepsilon$ is the spatial dimension. We will use dimensional regularisation and minimal subtraction [2] where space-time, $\mathrm{R}\times\mathrm{T}^3$, is extended to $\mathrm{R}\times\mathrm{T}^d$ [3]. Expanding eq. (2.3) in powers of p_0^2 and combining with the tree level and a tadpole contribution we find

$$S_{\text{eff}}(\text{1-loop, quadratic in } B) = \int \mathrm{d}t\left\{\frac{(d-1)^2}{d}\sum_k \frac{1}{|k|}\,\mathrm{Tr}\big(B_i^2\big) + \frac{1}{2}\left(\frac{L^3}{g_0^2} - \frac{2(7d+1)}{8d}\sum_k \frac{1}{|k|^3}\right)\mathrm{Tr}\big(\dot{B}_i^2\big) + \frac{(7d+1)}{32d}\sum_{l=0}\frac{(-1)^l}{4^l}\sum_k \frac{1}{|k|^{2l+5}}\,\mathrm{Tr}\left(\frac{\mathrm{d}^{l+2}B_i}{\mathrm{d}t^{l+2}}\right)^2\right\}. \tag{2.4}$$

The momentum sums are easily evaluated:

$$\sum_k \frac{1}{|k|^{2s}} = \left(\frac{L}{2\pi}\right)^{2s} a(2s), \tag{2.5}$$

where $a(2s)$ are lattice sums, tabulated for $d = 3$ in [10]. Only $a(3)$ has a pole at

TABLE 1
Coefficients for the effective potential (eqs. (2.16), (2.17) and (3.2)) and the effective hamiltonian (eqs. (3.1) and (3.3))

$\kappa_1 = -0.30104661$	$\alpha_1 = 2.1810429 \times 10^{-2}$
$\kappa_2 = -6.3319840 \times 10^{-3}$	$\alpha_2 = 7.5714590 \times 10^{-3}$
$\kappa_3 = 5.6289546 \times 10^{-4}$	$\alpha_3 = -1.1130266 \times 10^{-4}$
$\kappa_4 = -1.5687855 \times 10^{-3}$	$\alpha_4 = -2.1475176 \times 10^{-4}$
$\kappa_5 = 4.9676959 \times 10^{-5}$	$\alpha_5 = -1.2775652 \times 10^{-3}$
$\kappa_6 = -5.5172502 \times 10^{-5}$	$p = 1.059728073 \times 10^{-3}$
$\kappa_7 = -1.2423581 \times 10^{-3}$	$q = 2.844952587 \times 10^{-4}$
$\kappa_8 = -1.1130266 \times 10^{-4}$	$r = 2.533812424 \times 10^{-4}$
$\kappa_9 = -2.1475176 \times 10^{-4}$	
$\kappa_{10} = -1.2775652 \times 10^{-3}$	

$d = 3$, and using Lüscher's results [3] we find explicitly:

$$L^{-3}\sum_{k}\frac{1}{|k|^3} = \frac{-1}{2\pi^2(d-3)} + \frac{18a_2}{11} - \frac{1}{44\pi^2},$$

$$a_2 = \frac{22}{9(4\pi)^2}\left(\ln(\mu L)^2 - 0.409052802\right). \tag{2.6}$$

We now choose the renormalisation scale μ to be $1/L$, and write $g(L)$ for the renormalised coupling constant in the MS scheme. Thus:

$$\mathscr{L}(\text{1-loop, quadratic in } B) = \int \mathrm{d}\tau \left(2\kappa_1 \mathrm{Tr}\left(c_i^2\right) + \left(\frac{1}{g^2(L)} - 3\kappa_2 + \frac{1}{36\pi^2} \right) \mathrm{Tr}\left(\frac{\mathrm{d}c_i}{\mathrm{d}\tau} \right)^2 + \Delta\kappa\, \mathrm{Tr}\left(\left(\frac{\mathrm{d}^2 c_i}{\mathrm{d}\tau^2} \right)^2 \right) + \cdots \right), \tag{2.7}$$

where $c_i = LB_i$ is dimensionless, κ_1 and κ_2 are given in table 1, and

$$\Delta\kappa = -2.4285435\ldots \cdot 10^{-4},$$

$$\tau = t/L. \tag{2.8}$$

Note that the coefficients of the higher derivative terms are small, decaying as $(11/32l)/(2\pi)^{2l+1}$ for $\mathrm{Tr}[(\mathrm{d}/\mathrm{d}\tau)^l c_i]^2$. From now on we drop these terms, as well as any terms more than quadratic in c involving time derivatives. This is called the adiabatic approximation, and for higher powers of B it amounts to taking B constant in time, i.e., to calculating the effective potential.

For the one-loop result, instead of using Feynman graphs, we will expand the following well known result for the one-loop effective potential V_1:

$$\int_0^T \mathrm{d}t\, V_1(c) = \ln\Big[\det'\big(-D_\mu^2(B)\big)\Big/\det'\big(\mathscr{W}_{\mu\nu}(B)\big)^{1/2}\Big], \tag{2.9}$$

with $(D_\mu(B))^2$ the inverse ghost propagator and $\mathscr{W}_{\mu\nu}(B)$ the inverse vector propagator. The Fourier transforms of these inverse propagators are of the form $k_0^2\mathbf{1} + \boldsymbol{M}(\boldsymbol{k})$ with $\boldsymbol{M}$ a 3- or $3d$-dimensional matrix. Using zeta function regularisation and Poisson resummation

$$\sum_{Tk_0/2\pi\in Z} \mathrm{e}^{-k_0^2 s} = \frac{T}{\sqrt{4\pi s}} \sum_n \mathrm{e}^{-(nT)^2/4s} \overset{T\to\infty}{=} \frac{1}{2\sqrt{\pi s}} \int_0^T \mathrm{d}t \tag{2.10}$$

gives our result:

$$V_1(c) = \frac{L^3}{2g_0^2}\mathrm{Tr}\, F_{ij}^2(B) - \int_0^\infty \mathrm{d}s \frac{s^{-3/2}}{2\sqrt{\pi}}$$

$$\times\Big\{\tfrac{1}{2}\sum_{\boldsymbol{k}\neq\boldsymbol{0}} \mathrm{tr}\,\mathrm{Tr}\exp\Big(-s\big[\delta_{\mu\nu}(k_i + \mathrm{ad}\, B_i)^2 - 2i\,\mathrm{ad}\, F_{\mu\nu}(B)\big]\Big)$$

$$- \sum_{\boldsymbol{k}\neq\boldsymbol{0}} \mathrm{Tr}\exp\big(-s(k_i + \mathrm{ad}\, B_i)^2\big) - \tfrac{3}{2}(d-2)\Big\}. \tag{2.11}$$

Here

$$\mathrm{ad}\, B_i(\sigma^a) = -i\varepsilon_{abc}B_i^b\sigma_c,$$

$$F_{ij}(B) = i\big[B_i, B_j\big],$$

$$F_{0\mu} = F_{\nu 0} = 0. \tag{2.12}$$

Tr is the SU(2) trace in the adjoint representation, and tr is the space-time trace. We have subtracted a constant to make $V_1(B=0)=0$.

The graph expansion is now replaced by an expansion of the exponentials. Using

$$\int_0^\infty \mathrm{d}s \frac{s^{n-3/2}}{2\sqrt{\pi}} \mathrm{e}^{-sk^2} = \frac{2(2n-2)!}{(n-1)!4^n|\boldsymbol{k}|^{2n-1}}, \tag{2.13}$$

we find:

$$V_1 = \frac{(d-1)^2}{4d}\sum_k \frac{1}{|k|}\mathrm{Tr}\big((\mathrm{ad}\,B_i)^2\big) + \frac{1}{4}\left(\frac{L^3}{2g_0^2} - \sum_k \frac{1}{|k|^3}\right)\mathrm{Tr}\Big(\big(\mathrm{ad}\,F_{ij}(B)\big)^2\Big)$$

$$- \frac{(d-1)(d-6)}{16d}\sum_k \frac{1}{|k|^3}\mathrm{Tr}\big((\mathrm{ad}\,B_i)^2(\mathrm{ad}\,B_j)^2\big)$$

$$- \frac{5(d-1)}{16}\sum_k \frac{k_i k_j k_l k_m}{|k|^7}\mathrm{Tr}(\mathrm{ad}\,B_i \mathrm{ad}\,B_j \mathrm{ad}\,B_k \mathrm{ad}\,B_l)$$

$$- \tfrac{7}{48}\sum_k \frac{1}{|k|^5}\mathrm{Tr}\Big(\big[(\mathrm{ad}\,B_i)^2\big]^3\Big) - \tfrac{5}{48}\sum_k \frac{1}{|k|^5}\mathrm{Tr}\big((\mathrm{ad}\,B_i)^2 \mathrm{ad}\,B_j (\mathrm{ad}\,B_k)^2 \mathrm{ad}\,B_j\big)$$

$$+ \tfrac{1}{4}i\sum_k \frac{1}{|k|^5}\mathrm{Tr}\big(\mathrm{ad}\,F_{ij}(B)\mathrm{ad}\,F_{jk}(B)\mathrm{ad}\,F_{ki}(B)\big)$$

$$- \tfrac{5}{24}\sum_k \frac{1}{|k|^5}\mathrm{Tr}\Big(\big(\mathrm{ad}\,F_{ij}(B)\mathrm{ad}\,B_k\big)^2\Big) - \tfrac{1}{24}\sum_k \frac{1}{|k|^5}\mathrm{Tr}\Big(\big(\mathrm{ad}\,F_{ij}(B)\big)^2(\mathrm{ad}\,B_k)^2\Big)$$

$$+ \tfrac{35}{16}\sum_k \frac{k_i k_j k_k k_l}{|k|^9}\mathrm{Tr}\big((\mathrm{ad}\,B_m)^2 \mathrm{ad}\,B_i \mathrm{ad}\,B_j \mathrm{ad}\,B_k \mathrm{ad}\,B_l\big)$$

$$- \tfrac{21}{16}\sum_k \frac{k_i k_j k_k k_l k_m k_n}{|k|^{11}}\mathrm{Tr}(\mathrm{ad}\,B_i \mathrm{ad}\,B_j \mathrm{ad}\,B_k \mathrm{ad}\,B_l \mathrm{ad}\,B_m \mathrm{ad}\,B_n)$$

$$+ \mathrm{O}(B^8). \tag{2.14}$$

For terms of $\mathrm{O}(B^6)$ and higher the momentum sums converge and we have set $d = 3$. This expression can be simplified considerably by using a complete set of polynomials of even degree. One way is to write all the traces in terms of $M_{ij} = c_i^a c_j^a$, using $\mathrm{ad}\,F_{ij}(B) = i[\mathrm{ad}\,B_i, \mathrm{ad}\,B_j]$. However, the following complete set turns out to have physical significance:

$$\sum_{a=1}^{3} c_i^a c_i^a, \qquad i = 1,2,3;$$

$$\sum_{a=1}^{3} F_{ij}^a(c) F_{ij}^a(c), \qquad 3 \geqslant i > j \geqslant 1, \qquad F_{ij}^a(c) = -\varepsilon_{abd} c_i^b c_j^d;$$

$$(\det c)^2. \tag{2.15}$$

Note that $(\det c)^2$ must be included to determine the sign of $c_i^a c_j^a$, $(i \neq j)$. The final result using the tricks in appendix A, is

$$
\begin{aligned}
LV_1(c) = {} & \kappa_1 c_i^a c_i^a + \frac{1}{4}\left(\frac{1}{g^2(L)} - 3\kappa_2 + \frac{1}{18\pi^2}\right) F_{ij}^a(c) F_{ij}^a(c) \\
& + \kappa_3\left(3c_k^a c_k^a c_l^b c_l^b - 2F_{kl}^a(c) F_{kl}^a(c)\right) \\
& + \kappa_4\left(5c_k^a c_k^a c_k^b c_k^b - 3c_k^a c_k^a c_l^b c_l^b + 2F_{kl}^a(c) F_{kl}^a(c)\right) \\
& + \kappa_5 \sum_i \left(c_i^a c_i^a\right)^3 + \kappa_6 \sum_{i \neq j} c_i^a c_i^a \left(c_j^b c_j^b\right)^2 + \kappa_7 \prod_i c_i^a c_i^a \\
& + \kappa_8 F_{ij}^a(c) F_{ij}^a(c) c_k^b c_k^b + \kappa_9 \sum_{i \neq j} F_{ij}^a(c) F_{ij}^a(c) c_j^b c_j^b + \kappa_{10} (\det c)^2 + \mathrm{O}(c^8) .
\end{aligned}
\tag{2.16}
$$

Terms up to and including fourth order arise exactly as in Lüscher's calculation. In terms of lattice sums, the new κ_i, $i = 5, \ldots, 10$ are:

$$
\begin{aligned}
\kappa_5 &= \left(-\tfrac{1}{2}p + \tfrac{35}{8}q - \tfrac{21}{8}r\right), \\
\kappa_6 &= \left(\tfrac{23}{8}p - \tfrac{455}{16}q + \tfrac{315}{16}r\right), \\
\kappa_7 &= \left(-\tfrac{117}{4}p + 315q - \tfrac{945}{4}r\right), \\
\kappa_8 &= \left(\tfrac{583}{96}p - \tfrac{1029}{16}q + \tfrac{189}{4}r\right), \\
\kappa_9 &= \left(-\tfrac{1407}{96}p + \tfrac{4865}{32}q - \tfrac{441}{4}r\right), \\
\kappa_{10} &= \left(-\tfrac{39}{4}p + \tfrac{1407}{16}q - 63r\right), \\
p &= \frac{1}{(2\pi)^5} \sum_{n \in Z^3} \frac{1}{|n|^5}, \qquad q = \frac{1}{(2\pi)^5} \sum_{n \in Z^3} \frac{n_1^4}{|n|^9}, \\
r &= \frac{1}{(2\pi)^5} \sum_{n \in Z^3} \frac{n_1^6}{|n|^{11}} .
\end{aligned}
\tag{2.17}
$$

The numerical values are given in table 1.

Rescaling the fields by

$$c \to g^{2/3}\left(1+\left(\kappa_2-\frac{1}{72\pi^2}\right)g^2\right)c \tag{2.18}$$

would reproduce Lüscher's result for the quadratic and quartic parts. However, this rescaling would make the vacuum valley coordinates depend on g, so we do not incorporate it. A useful feature of these coordinates is that the vacuum valley is neatly parameterised. The vacuum valley in Lüscher's effective hamiltonian is the set of *abelian* spatially constant vector potentials. Previously [4], we parameterised this set by first fixing the gauge, which was not possible near the origin $c_i^a = 0$. In our new coordinates, however, the vacuum valley is uniquely defined by $F_{ij}^2(c) = 0$ for all i, j (which implies $(\det c)^2 = 0$). Thus we can introduce gauge invariant vacuum valley coordinates

$$C_i = \sqrt{\sum_{a=1}^{3} c_i^a c_i^a} = \frac{1}{L^4}\sqrt{\sum_{a=1}^{3}\int \mathrm{d}^3x\,\mathrm{d}^3x'\,A_i^a(x)A_i^a(x')}\,. \tag{2.19}$$

The remaining coordinates are angles, defined by choosing spherical coordinates (C_i, θ_i, ϕ_i) for the vectors $\boldsymbol{c}_i = (c_i^1, c_i^2, c_i^3)$; explicitly:

$$\left(c_i^1, c_i^2, c_i^3\right) = C_i(\cos\phi_i\sin\theta_i, \sin\phi_i\sin\theta_i, \cos\theta_i)\,. \tag{2.20}$$

It is thus convenient to think of the nine c_i^a as being three SO(3) vectors with labels $i = 1, 2, 3$. An intuitive way to describe the vacuum valley is to say that the three vectors $\boldsymbol{c}_i$ are all lined up, their common direction being an overall gauge freedom.

We can now easily improve our result for the effective potential in two ways with very little extra work. First, we can extend part of the one-loop result for $V_1(c)$ to infinite order in C_i. Observe that the one-loop effective potential along the vacuum valley is known to infinite order [3, 4]:

$$\hat{V}_1(\curlyvee, C) = \frac{4}{\pi^2 L}\sum_{\boldsymbol{n}\neq\boldsymbol{0}}\frac{\sin^2\left(\boldsymbol{n}\cdot\frac{1}{2}\boldsymbol{C}\right)}{(\boldsymbol{n}^2)^2}\,. \tag{2.21}$$

$\hat{V}_1$ differs from V_1 in that more modes (the spatially constant but non-vacuum modes) have been integrated out. It was calculated by Lüscher [3] using gauge-fixed coordinates, and as we have discussed extensively previously [4], is related to V_1 by

$$V_1(\boldsymbol{C}) \equiv V_1\left(c, F_{ij}^2(c) = 0\right) = \hat{V}_1(\curlyvee, C) - \frac{2}{L}|\boldsymbol{C}|\,. \tag{2.22}$$

Note the change in notation from ref. [4], where V_1 was denoted by V_1' and

$\hat{V}_1(\mathscr{V}, C)$ by $V_1(C)$. We can thus find the higher powers of C in V_1. Also, Taylor expanding both sides of this equation gives a consistency check on our calculations. We find the following new relations involving the coefficients a_n and c_n defined in ref. [4] and the Riemann zeta-function ζ [19].

$$\kappa_5 = -\frac{1}{180\pi}\sum_{n=1}^{\infty} n^6 a_n,$$

$$4\kappa_6 + 30\kappa_5 = \frac{\zeta(5)}{4\pi^5} + \frac{1}{3\pi}\sum_{n=1}^{\infty} n^4 c_n,$$

$$\kappa_7 + 18\kappa_6 + 45\kappa_5 = 0. \tag{2.23}$$

The last identity follows from

$$\left(\frac{\partial^2}{\partial C_i^2}\right)^2 V_1\big(c, F_{ij}^2(c) = 0\big) \equiv \Delta^2 V_1(\boldsymbol{C}) = 2/\pi^2. \tag{2.24}$$

A second improvement we can easily make is to calculate the two-loop effective potential along the vacuum valley. Since the B_i mutually commute when $F_{ij}^2 = 0$, one can diagonalise the propagators. Choose for convenience $B_i = B_i^3\sigma_3/2 = C_i\sigma_3/2L$. The Feynman rules of ref. [9] can again be used. There, the two-loop result was calculated in terms of parameters $\lambda^{(a)}$, where (a) is an adjoint SU(2) index. We can apply the result here by using the following trick: take the SU(2) basis $a \in \{+, -, 3\}$ with

$$\sigma_{\pm} = \sqrt{\tfrac{1}{2}}(\sigma_1 \pm i\sigma_2), \qquad \sigma_3 = \sigma_3,$$

$$\lambda^{(+)} = \boldsymbol{C}/2\pi,$$

$$\lambda^{(-)} = -\boldsymbol{C}/2\pi,$$

$$\lambda^{(3)} = \boldsymbol{0}. \tag{2.25}$$

Thus we find

$$V_2(\boldsymbol{C}) \equiv V_2\big(c, F_{ij}^2(c) = 0\big) = \tfrac{1}{64}g^2 L \sum_{\substack{a \neq b \\ a,b=\{+,-,3\}}} \Delta V_1(2\pi\lambda^{(a)})\,\Delta V_1(2\pi\lambda^{(b)})$$

$$= \tfrac{1}{32}g^2 L\Big[\big(\Delta V_1(\boldsymbol{C})\big)^2 + 2\,\Delta V_1(\boldsymbol{C})\,\Delta V_1(\boldsymbol{0})\Big]. \tag{2.26}$$

In summary, we know the effective potential to two-loop and to all orders in the fields if we restrict ourselves to the vacuum valley, whereas away from the vacuum

valley we have calculated the effective potential the hard way to sixth order in the fields.

Since the potential is shaped so the wave function concentrates near the vacuum valley, it makes intuitive sense to approximate the potential accurately along the valley, and use a simpler approximation for deviations from the valley. Roughly speaking, the transverse term serves mainly to concentrate the wave function near the valley. It turns out that a sixth-order vacuum-valley potential with the lowest (fourth) order transverse piece captures enough of the structure to give good results. A weaker approximation along the vacuum valley gets the barrier height wrong, so that tunneling sets in at the wrong value of g.

3. Reduction to a vacuum valley problem

In this section we reexamine the question of writing Lüscher's effective hamiltonian as an effective hamiltonian for just the vacuum-valley cordinates C_i. In previous work [4] we emphasized the severe obstacles to this, because the modes to be integrated out had extremely non-adiabatic behaviour near $\boldsymbol{C} = 0$. Thus, although we could find an effective hamiltonian for $\boldsymbol{C}$ away from $\mathbf{0}$, special arrangements had to be made near the origin. In our new coordinates, the behaviour is rather different, and requires some new discussion.

We are interested in this issue, because it determines the accuracy of some of the boundary conditions we deduce in sect. 4.

Because Lüscher's hamiltonian is similar to a three-particle quantum mechanics problem, we will often use the notation r_i for the vacuum valley coordinate C_i. Also, we write $\boldsymbol{r}_i = (c_i^1, c_i^2, c_i^3)$, and to avoid confusion we denote the triple (r_1, r_2, r_3) by $\boldsymbol{C}$. Compared to ref. [4], our new coordinates make the following discussion much simpler.

Lüscher's effective hamiltonian as extended in sect. 2 can be written as:

$$H_{\text{eff}} = -\frac{1}{2L}\left(\frac{1}{g^2} + \alpha_1\right)^{-1} \frac{\partial^2}{(\partial c_i^a)^2} + V_{\text{T}}(c) + V_l(c), \tag{3.1}$$

where $\alpha_1 = 1/36\pi^2 - 3\kappa_2$. The "radial" or "longitudinal" effective potential $V_l(c)$ is independent of the angular variables. If $V_{l,i}$ is the i-loop contribution,

$$V_l(c) = V_{l,1}(c) + V_{l,2}(c) + \cdots,$$

$$V_{l,1}(c) = \hat{V}_1(\mathscr{V}, C) - 2|\boldsymbol{C}|/L,$$

$$V_{l,2}(c) = \frac{g^2 L}{32}\left(\frac{6\kappa_1}{L} + \frac{\partial^2 V_{l,1}(c)}{(\partial \boldsymbol{C})^2}\right)^2 - \frac{9g^2\kappa_1^2}{8L}. \tag{3.2}$$

We normalise so that $V_l(0)=0$, a fact to be kept in mind when analyzing vacuum energies. Similarly, $V_T(c)=V_{T,1}(c)+\cdots$ is the transverse part of the effective potential, vanishing along the vacuum valley:

$$L\cdot V_{T,1}(c)=\frac{1}{4}\left(\frac{1}{g^2}+\alpha_2\right)F^a_{ij}F^a_{ij}+\alpha_3\left(F^a_{ij}F^a_{ij}\right)c^b_k c^b_k$$
$$+\alpha_4\sum_{i,j}F^a_{ij}F^a_{ij}c^b_j c^b_j+\alpha_5(\det c)^2+\cdots, \tag{3.3}$$

with $\alpha_2=1/(18\pi^2)-3\kappa_2+8(\kappa_4-\kappa_3)$, $\alpha_3=\kappa_8$, $\alpha_4=\kappa_9$ and $\alpha_5=\kappa_{10}$. The numerical values for α_i are also given in table 1.

We decompose the wave function by writing it in the following way:

$$\Psi(c)=\sum_{n=1}^{\infty}(r_1r_2r_3)^{-1}\Phi^{(n)}(\boldsymbol{C})\chi^{(n)}_{[C]}(\theta_i,\phi_i), \tag{3.4}$$

where the transverse wave functions $\chi^{(n)}_{[C]}(\theta_i,\phi_i)$ are eigenstates of the "transverse hamiltonian,"

$$H_{tr}\chi^{(n)}_{[C]}\equiv\left(\frac{1}{L}\left(\frac{1}{g^2}+\alpha_1\right)^{-1}\sum_{i=1}^{3}\frac{\boldsymbol{L}_i^2}{2r_i^2}+V_T(c)\right)\chi^{(n)}_{[C]}$$
$$=V^{(n)}_{tr}(\boldsymbol{C})\chi^{(n)}_{[C]}. \tag{3.5}$$

Here $\boldsymbol{L}_i$ is the standard 1-particle angular momentum operator. H_{tr} is obtained by treating the r_i in H_{eff} as fixed parameters. The decomposition can be thought of as using a coordinate representation for the r_i and an energy representation for the angles. Thus $\Psi(c)$ is completely equivalent to an infinite number of vacuum-valley wave functions $\Phi^{(n)}(\boldsymbol{C})$. For simplicity we normalise $\chi^{(n)}_{[C]}$ using $d\Omega=\sin\theta\,d\theta\,d\phi$ so that at fixed r_i

$$\langle\chi^{(n)}_{[C]}|\chi^{(m)}_{[C]}\rangle=\int d\Omega_1\,d\Omega_2\,d\Omega_3\,\chi^{(n)*}_{[C]}(\theta_i,\phi_i)\chi^{(m)}_{[C]}(\theta_i,\phi_i)=\delta_{n,m}. \tag{3.6}$$

Note that the eigenvalues of H_{tr} form an increasing sequence of $\boldsymbol{C}$-dependent "effective potentials."

With this decomposition, the eigenvalue equation for H_{eff} can be rewritten as [4, 7]:

$$\left[-\frac{g^2}{2L(1+g^2\alpha_1)}\left(\nabla^{nm}(\boldsymbol{C})\right)^2+\left(V_l(\boldsymbol{C})+V^{(n)}_{tr}(\boldsymbol{C})\right)\delta_{nm}\right]\Phi^{(m)}(\boldsymbol{C})$$
$$=E\Phi^{(n)}(\boldsymbol{C}). \tag{3.7}$$

$\nabla^{nm}(\boldsymbol{C})$ is a "covariant derivative"

$$\nabla^{nm}(\boldsymbol{C}) = \delta^{nm}\frac{\partial}{\partial \boldsymbol{C}} + \langle \chi^{(n)}_{[C]} | \frac{\partial}{\partial \boldsymbol{C}} | \chi^{(m)}_{[C]} \rangle$$

$$\equiv \delta^{nm}\frac{\partial}{\partial \boldsymbol{C}} - \boldsymbol{A}^{nm}(\boldsymbol{C}). \tag{3.8}$$

The radial factor $(r_1 r_2 r_3)^{-1}$ included in (3.4) produces a simple normalisation:

$$\langle \Psi | \tilde{\Psi} \rangle = \sum_{n=1}^{\infty} \int_0^{\infty} \mathrm{d}^3 C \, \Phi^{(n)}(\boldsymbol{C}) * \tilde{\Phi}^{(n)}(\boldsymbol{C}). \tag{3.9}$$

Now, an effective hamiltonian for the vacuum valley $\mathscr{V}$ will be well defined if the adiabatic approximation, obtained by truncating eq. (3.7) to $n = m = 1$, is accurate. Therefore either of two conditions is sufficient: if $\boldsymbol{A}^{nm}(\boldsymbol{C})$ is small, the $n = 1$ sector decouples from higher sectors, whereas if $\Delta E^{(2)} = V^{(2)}_{\mathrm{tr}}(\boldsymbol{C}) - V^{(1)}_{\mathrm{tr}}(\boldsymbol{C})$ is large compared to the energy $E \sim g^{2/3}/L$ we are working at, the higher Φ's are small and irrelevant. Let $\overline{\Delta E}^{(2)} = \inf_{\boldsymbol{C}} \Delta E^{(2)}$ be the minimum transverse energy gap. In many problems, $E/\overline{\Delta E}^{(2)}$ is a positive power of g (e.g., for the non-zero momentum modes integrated out to obtain Lüscher's effective hamiltonian one has $E/\overline{\Delta E}^{(2)} = \mathrm{O}(g^{2/3})$). In such cases the adiabatic approximation improves as $g \to 0$, and can be incorporated as a controlled expansion in g. However, as we will see shortly, because the transverse fluctuations are now quartic, both $L \cdot E$ and $L \cdot \overline{\Delta E}$ are $\mathrm{O}(g^{2/3})$, and the adiabatic approximation in perturbation theory is not directly controlled by an expansion in g. This is why *a priori* one cannot work entirely within the vacuum valley.

To see exactly where the nonadiabatic behaviour is, we turn to investigating the transverse hamiltonian H_{tr} in eq. (3.5), and it suffices to consider just the leading order in g to exhibit the relevant features. We thus wish to solve the hamiltonian (we have put $L = 1$ for convenience)

$$H_{\mathrm{tr}} = \frac{g^2}{2}\sum_i \frac{\boldsymbol{L}_i^2}{r_i^2} + \frac{1}{2g^2}\sum_{i>j}\left(r_i^2 r_j^2 - (\boldsymbol{r}_i \cdot \boldsymbol{r}_j)^2\right), \tag{3.10}$$

where $\boldsymbol{L}_i$ is the standard 1-particle angular momentum operator. A gauge transformation acts on each "particle" as a rotation (not to be confused with a space rotation, which mixes the r_i). Gauge invariance is therefore equivalent to constraining the total "angular momentum" to be zero:

$$\boldsymbol{L} = \boldsymbol{L}_1 + \boldsymbol{L}_2 + \boldsymbol{L}_3 = \boldsymbol{0}. \tag{3.11}$$

Note that an expansion in g is deceptive since by rescaling $r_i = g^{2/3}\hat{r}_i$ one can scale $H_{\rm tr}$ to depend on g by an overall factor:

$$H_{\rm tr} = g^{2/3}\left(\sum_i \frac{\boldsymbol{L}_i^2}{2\hat{r}_i^2} + \tfrac{1}{2}\sum_{i>j}\left[\hat{r}_i^2\hat{r}_j^2 - (\boldsymbol{r}_i\cdot\boldsymbol{r}_j)^2\right]\right). \tag{3.12}$$

Thus the transverse energy is $O(g^{2/3})$, and the correct expansion parameter is $\hat{r} = r/g^{2/3}$. One easily derives the following explicit form:

$$g^{-2/3}H_{\rm tr} = \sum_i \frac{\boldsymbol{L}_i^2}{2\hat{r}_i^2} + \tfrac{1}{2}\sum_{i>j}\hat{r}_i^2\hat{r}_j^2\big[\sin^2\theta_i\sin^2\theta_j\sin^2(\phi_i-\phi_j)$$

$$+\sin^2(\theta_i-\theta_j) + \sin(2\theta_i)\sin(2\theta_j)\sin^2\big(\tfrac{1}{2}(\phi_i-\phi_j)\big)\big]. \tag{3.13}$$

This is too difficult to solve in general, so we look at limiting cases. First, if all $\hat{r}_i \gg 1$, one can consider fluctuations about the vacuum valley.

Using the gauge invariance we write $\theta_i = \frac{1}{2}\pi + x_i/\hat{r}_i$, $\phi_i = y_i/\hat{r}_i$ to get approximately

$$g^{-2/3}H_{\rm tr} \simeq H(x_i) + H(y_i),$$

$$H(x_i) = -\frac{1}{2}\frac{\partial^2}{\partial x_i^2} + V(x_i),$$

$$V(x_i) = \tfrac{1}{2}\sum_{i>j}\hat{r}_i^2\hat{r}_j^2\left(\frac{x_i}{\hat{r}_i} - \frac{x_j}{\hat{r}_j}\right)^2. \tag{3.14}$$

To determine the spectrum one diagonalises the hessian of the potential V:

$$\frac{\partial^2 V}{\partial x_i\,\partial x_j} = \begin{pmatrix} \hat{r}_2^2+\hat{r}_3^2 & -\hat{r}_1\hat{r}_2 & -\hat{r}_1\hat{r}_3 \\ -\hat{r}_1\hat{r}_2 & \hat{r}_1^2+\hat{r}_3^2 & -\hat{r}_2\hat{r}_3 \\ -\hat{r}_1\hat{r}_3 & -\hat{r}_2\hat{r}_3 & \hat{r}_1^2+\hat{r}_2^2 \end{pmatrix}, \tag{3.15}$$

which is easily seen to have two degenerate eigenvectors with eigenvalue $\lambda = \sum_i \hat{r}_i^2$ and one zero eigenvalue with eigenvector $(\hat{r}_1, \hat{r}_2, \hat{r}_3)$. The zero eigenvalue is due to the gauge invariance and should be ignored, so the transverse spectrum is

$$V_{\rm tr}^{(n)} = \tfrac{1}{2}|\boldsymbol{C}|\left(\sum_{i=1}^{4}(2n_i+\tfrac{1}{2})\right)$$

$$= 2|\boldsymbol{C}|, 3|\boldsymbol{C}|, 4|\boldsymbol{C}|, \ldots \qquad C_i \gg g^{2/3}. \tag{3.16}$$

Thus we reproduce the one-loop result obtained in previous gauge-fixed analysis [3,4]. Since $V_{\rm tr}^{(2)} - V_{\rm tr}^{(1)} \gg E \sim g^{2/3}$, the adiabatic approximation holds in this region.

Next we go to the opposite limit of all $\hat{r}_i$ small. In that case the kinetic term clearly dominates, which means each "particle" will be in the lowest angular momentum state. Hence to lowest order the transverse energy is given by the potential of $H_{\rm tr}$ averaged over the sphere:

$$V_{\rm tr}^{(1)} = \frac{g^{2/3}}{3} \sum_{i>j} \hat{r}_i^2 \hat{r}_j^2 = \frac{1}{3g^2} \sum_{i>j} r_i^2 r_j^2 . \tag{3.17}$$

To find excited states, note that gauge invariance, i.e., zero total angular momentum, requires

$$l_1 + l_2 \geqslant l_3 , \qquad l_2 + l_3 \geqslant l_1 , \qquad l_3 + l_1 \geqslant l_2 . \tag{3.18}$$

Thus, in the even parity sector (see sect. 5), the first excited state will correspond to $l_1 = l_2 = 2$, $l_3 = 0$ (assuming $\hat{r}_3 < \hat{r}_2 \leqslant \hat{r}_1$), giving

$$V_{\rm tr}^{(2)} = \frac{3g^{2/3}}{\hat{r}_1^2} + \frac{3g^{2/3}}{\hat{r}_2^2} \qquad \left(C_i \ll g^{2/3}\right). \tag{3.19}$$

The surprising conclusion then, is that the adiabatic approximation is also good if all $\hat{r}_i \ll 1$. This is the first indication that our new coordinates are rather different from the ones in ref. [4]. A second surprise is that exactly the same reasoning holds if only two of the $\hat{r}_i$ are small, since if two of the l_i are zero, the conditions (3.18) force the third one to be small too. Thus the effective potential is still given by (3.17), which vanishes if two of the $\hat{r}_i$ are zero. A region with two $\hat{r}_i$ small is a minimum action tunneling path for the system, called a pinchon [4,8], and it is very surprising to find a vanishing effective potential here, because in ref. [4], we claimed this effective potential was $2|\boldsymbol{C}|$ everywhere sufficiently far from $|\boldsymbol{C}| = 0$. Indeed, a second peculiarity is that, since the pinchons are on the boundary of the vacuum valley cube, the wave function vanishes there, as claimed in the introduction. To resolve this dilemma, note that the region $r_i \ll g^{2/3}$ where this approximation is valid actually vanishes as $g \to 0$, while the region $r_i \gg g^{2/3}$ where the expected form (3.16) is valid actually increases. In sect. 7 we give convincing numerical evidence that between these two regions is a region where the adiabatic approximation breaks down: $V_{\rm tr}^{(2)}$ and $V_{\rm tr}^{(1)}$ come reasonably close, and $\langle \chi_{[C]}^{(0)} | \partial/\partial \hat{r}_i | \chi_{[C]}^{(k)} \rangle$ is no longer small for $i = 1$ or 2. The net effect of this non-adiabatic region, which has zero support as $g \to 0$, is apparently to replace the vanishing condition on the wave function with a vanishing condition on its derivative. We will not try to prove this analytically, being satisfied in this paper with the numerical evidence, and the fact that we can verify our semiclassical formula.

The point of this section, then, is to observe that in these new coordinates, the region of non-adiabatic behaviour is not confined to very near the well. Thus, to use the boundary conditions we are about to derive, we need to check explicitly, a posteriori, whether the adiabatic approximation is sufficiently accurate. We will do this in sect. 7.

4. Boundary conditions and Gribov ambiguities

Gribov ambiguities [11] arise in non-perturbative discussions when one chooses gauge-fixed coordinates for configuration space. At some finite distance from the chosen origin, the tangent planes of the gauge orbit and the coordinate hypersurface can partially overlap. Beyond this point, in general, Gribov copies are formed, and the choice of gauge invariant coordinates is no longer uniquely determined by the gauge fixing procedure.

The Gribov horizon is the set of configurations where the copies are first formed, and is uniquely specified by the fact that at least one non-zero tangent vector to the gauge orbit is tangent to the coordinate plane. Equivalently, these points have a larger isotropy subgroup (the set of gauge transformations which leave that point invariant) than neighbouring points, and this is where the Faddeev-Popov determinant vanishes (or acquires an additional zero). It is imperative to note that if the set of gauge-invariant configurations $\mathscr{A}/\mathscr{G}$ is topologically non-trivial ($\mathscr{A}$ the set of all vector potentials), Gribov ambiguities cannot be avoided [12] in a linear gauge on a compact manifold, including the torus [13]. On the other hand, the same non-triviality causes the instantons whose effects dominate any non-perturbative analysis. Thus any attempt to add instanton effects to a perturbative analysis is bound to introduce the Gribov problem as well [15].

Let us therefore state unambiguously where in our analysis this problem arises. For this we will closely follow the Coulomb gauge hamiltonian formulation [16], used by Lüscher to obtain the effective hamiltonian. As he noted, the Faddeev-Popov determinant arises in the measure for configuration space. Two wave functionals $\Psi[A]$ and $\Theta[A]$, being gauge invariant, are well defined on $\mathscr{A}/\mathscr{G}$, and

$$\langle \Psi | \Theta \rangle = \int_{\mathscr{A}} \mathscr{D}A \Psi[A]^* \Theta[A]$$

$$= \int_{\mathscr{A}/\mathscr{G}} \mathscr{D}\tilde{A} \rho(\tilde{A}) \Psi[\tilde{A}]^* \Theta[\tilde{A}], \tag{4.1}$$

where $\tilde{A}$ satisfies the Coulomb gauge, and

$$\rho(\tilde{A}) = \det'\big(-\partial_k D_k(\tilde{A})\big). \tag{4.2}$$

The zero momentum modes are omitted in the functional determinant, and $D_k(\tilde{A})$ is the covariant derivative. Hence ρ is the measure for $\mathscr{A}/\mathscr{G}$, with its zeros constituting the Gribov horizon.

Now, the crucial point is that in perturbation theory the wave functional is rescaled with $\rho^{1/2}$

$$\hat{\Psi}[\tilde{A}] \equiv \rho(\tilde{A})^{1/2}\Psi[\tilde{A}] \tag{4.3}$$

to obtain a trivial integration measure. Therefore the new rescaled wave function *vanishes* at the Gribov horizon.

For SU(2) Yang-Mills on the torus, one easily verifies that $\rho(\tilde{A}) = 0$ if $A_i = (2\pi n_i/L)\sigma^a s_a/2$ for at least one i, with $n_i \in Z$ and $s^2 = 1$. (Take an eigenvector with $k_i = \pm 2\pi n_i/L$ and the other components of k zero.)

Thus $\hat{\Psi}[\tilde{A}]$ (and therefore presumably $\Psi(c)$) vanishes linearly in $2\pi n_i - r_i$ at $r_i = 2\pi n_i$ for any i.

Finally, recalling that we define $\Phi^{(n)}(\boldsymbol{C})$ in terms of $\Psi(c)$ with a factor $(r_1 r_2 r_3)$ factored out, we conclude that $\Phi^{(n)}(\boldsymbol{C})$ vanishes at the boundary of $\mathscr{V} = [0, 2\pi]^3$. Note that these boundary conditions are all caused by coordinate singularities.

Having shown that the wave function vanishes at the surface of $\mathscr{V}$, and thus in particular at the corners where the perturbative vacua occur, we turn our attention to the configurations midway between two perturbative vacua. Consider the gauge transformations

$$g_n(x) = \exp\left(-i\pi \frac{\boldsymbol{n}\cdot\boldsymbol{x}}{L}\sigma_a s^a\right), \tag{4.4}$$

where s^a is an arbitrary unit vector. It transforms the vector potential $\boldsymbol{A}$ into

$$g_n(x) A_i g_n^{-1}(x) + \frac{2\pi n_i}{L}\frac{\sigma_a s^a}{2}. \tag{4.5}$$

Take A_i abelian, and choose s such that $A_i = -(r_i/L)\sigma_a s^a/2$. Applying g_n gives $((2\pi n_i - r_i)/L)\sigma_a s^a/2$, so that in our gauge invariant coordinates,

$$r_i \to 2\pi n_i - r_i. \tag{4.6}$$

Thus if $n_i \in \{0, 1\}$, eq. (4.5) maps $\mathscr{V}$ into itself. Since g_n is a homotopically non-trivial gauge transformation, a wave functional $\Psi(A)$ with definite electric flux satisfies

$$\Psi_e({}^{g_n}A) = (-1)^{n\cdot e}\Psi_e(A), \tag{4.7}$$

which implies:

$$\hat{\Psi}_e({}^{g_n}A) = (-1)^{n\cdot e}\left(\frac{\rho({}^{g_n}A)}{\rho(\tilde{A})}\right)^{1/2}\hat{\Psi}_e(\tilde{A}). \tag{4.8}$$

From this we easily see that when A is restricted to the vacuum valley (where we can suppress the overall factor $\sigma_a s^a/2$),

$$\hat{\Psi}_e(2\pi\boldsymbol{n}-\boldsymbol{r}) = (-1)^{\boldsymbol{n}\cdot\boldsymbol{e}} \left(\frac{\rho(2\pi\boldsymbol{n}-\boldsymbol{r})}{\rho(\boldsymbol{r})} \right)^{1/2} \hat{\Psi}_e(\boldsymbol{r}). \tag{4.9}$$

Hence if $e_i = 1$ we conclude that on the vacuum valley, the wave function vanishes at $r_i = \pi$. Unfortunately, we are interested in the wave function $\Psi(c)$ for Lüscher's effective hamiltonian, which is not simply a restriction of the full wave function. We need to project onto the constant modes as prescribed by Bloch perturbation theory. This projection is only defined perturbatively, and we would need it to infinite order to find an exact boundary condition at $r_i = \pi$. This is beyond our capabilities. Nevertheless, (4.9) motivates us to look for a set of boundary conditions at $r_i = \pi$. For $e_i = 1$, the conclusion that the wave function vanishes at $r_i = \pi$ should survive the projection, so the real issue is the $e_i = 0$ boundary condition.

A point we have ignored so far is that Lüscher's effective hamiltonian breaks down as one approaches the Gribov horizon at $r_i = 2\pi$, because some of the higher momentum modes that have been integrated out become quartic. A way to circumvent this is to adapt an idea discussed by Nahm [14], that an alternative way to understand Gribov ambiguities is as a need for different coordinate patches in $\mathscr{A}/\mathscr{G}$, and transition functions to connect the coordinates in the overlap region of two such patches. As was advocated in our previous work [4], one centers a coordinate patch at each of the eight corners of the vacuum valley $\mathscr{V} = [0, 2\pi]^3$, and derives Lüscher's hamiltonian in the zero momentum (but for $2\pi\boldsymbol{n} \neq \boldsymbol{0}$, not necessarily constant) modes. Explicitly:

$$c_i^{(\boldsymbol{n})} = \frac{1}{L^3} \int_{\mathrm{T}^3} \mathrm{d}^3x \left({}^{g_{\boldsymbol{n}}^{-1}} A(x) \right). \tag{4.10}$$

By taking $A(x)$ in the vacuum valley, we conclude that $C_i^{(\boldsymbol{n})}$ is to be identified with $2\pi n_i - C_i^{(\boldsymbol{0})}$, where

$$C_i^{(\boldsymbol{n})} = \sqrt{2\,\mathrm{Tr}\left(\left(c_i^{(\boldsymbol{n})} \right)^2 \right)}\,. \tag{4.11}$$

For the remaining coordinates in each patch, we can use angular coordinates just as for $\boldsymbol{n} = \boldsymbol{0}$. Next, note that the ground state $\chi^{(1)}_{[C]}$ for the fluctuations transverse to the vacuum valley is unique, and a smooth function of r_i. If we assume for the moment that all of the wave function is in this transverse ground state, then $\Phi^{(1)}(\boldsymbol{C}^{(\boldsymbol{n})})$ defined in the patch at corner $2\pi\boldsymbol{n}$ must be identified with $\Phi^{(1)}(\boldsymbol{C}^{(\boldsymbol{0})})$. Note that the factor $(r_1 r_2 r_3)^{-1}$ included in the definition of $\Phi^{(i)}(\boldsymbol{C})$ (eq. (3.4)) again proves essential, because otherwise the measure on $\mathscr{V}$ would not be differentiable.

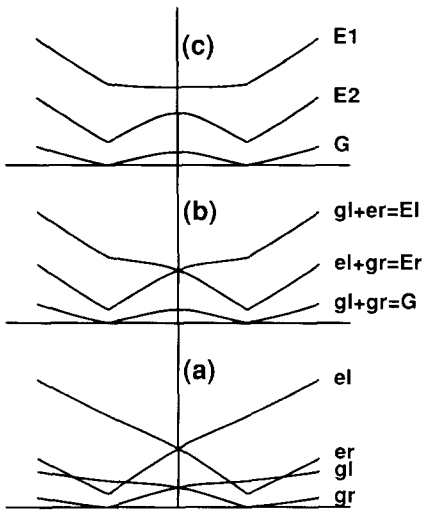

Fig. 2. Schematic illustration of avoidance of level crossing. We consider two transverse modes, and plot the "1-particle" energy levels in fig. 2a. For the transverse mode that becomes quartic to the right (left) we give the ground state gr (gl) and the first excited state er(el). In fig. 2b the total energies due to the transverse modes are plotted, without incorporating off-diagonal coupling. Fig. 2c shows the effect this off-diagonal coupling has on the level crossing of the states El and Er of fig. 2b. In fig. 2c, $E1$ and $E2$ are obtained in this simple example as the eigenvalues of the 2×2 matrix with Er and El on the diagonal and 1 off the diagonal.

Thus we find the following symmetry properties:

$$\Phi^{(1)}(2\pi n_i - r_i) = (-1)^{n \cdot e} \Phi^{(1)}(r_i). \tag{4.12}$$

The situation is more complicated if some of the wavefunction is in excited transverse states, since symmetry (eq. (4.5)) dictates a degeneracy in the excited transverse energies at $r_i = \pi$. In general this means an excited zero-momentum transverse state in one patch can become a non-zero momentum excited transverse state in another patch (see fig. 2b). This would lead to more complicated boundary conditions, because the latter were integrated out in Lüscher's effective hamiltonian. However, we do not expect this problem to be too severe, because if we take into account the off-diagonal coupling between transverse levels (by terms analogous to A_{nm}), we see that in general this problem is avoided (see fig. 2c). A simple example demonstrates this effect. Take a two-level system with hamiltonian

$$H = \begin{pmatrix} \lambda & g \\ g & -\lambda \end{pmatrix}. \tag{4.13}$$

At $g = 0$, the energy levels as a function of λ cross, whereas for $g \neq 0$ they do not come closer in energy than $\Delta E = 2g$.

To summarise, for small g we expect the boundary condition to be good because most of the wave function is in the transverse groundstate, whereas at large g we expect no level crossings between zero and non-zero momentum ground states. Thus as long as the latter *can* be integrated out, no inconsistencies arise. In that case, however, since transverse excited states are populated, we should demand that both $\Phi^{(i)}$ and $(\nabla\Phi)^{(i)}$ be continuous across the boundary separating the two coordinate patches, to ensure a continuous energy density. Hence, using the symmetries (4.7), we find the following boundary conditions at $r_i = \pi$:

$$(\nabla_i)^{1-e_i}\Phi = 0\,, \tag{4.14}$$

which is easily seen to be equivalent to:

$$\left(\frac{\partial}{\partial r_i}\right)^{1-e_i}(r_i\Psi(c)) = 0\,. \tag{4.15}$$

These are the boundary conditions used for the Rayleigh-Ritz analysis. There is an additional argument why in eq. (4.14) the "covariant derivative" instead of the ordinary derivative should appear: one is free to choose the phase of $\chi^{\{n\}}_{[C]}$, even if it depends on C. Eq. (4.14) gives a condition independent of this choice.

After the Rayleigh-Ritz calculation is done, we need to test whether at the boundary most of the wave function is indeed concentrated in the lowest transverse state. We can calculate the following quantity:

$$f_i = \lim_{r_i\to\pi} \frac{\int_0^\pi\int_0^\pi \mathrm{d}r_j\,\mathrm{d}r_k |\Phi^{(1)}(C)|^2}{\int_0^\pi\int_0^\pi \mathrm{d}r_j\,\mathrm{d}r_k \sum_{l=1}^{\infty} |\Phi^{(l)}(C)|^2} \qquad (i\neq j\neq k)\,, \tag{4.16}$$

which is the fraction of the wavefunction actually in the lowest transverse state, at the boundary $r_i = \pi$. We will verify in sect. 7 that $1 - f_i$ becomes smaller for smaller g, indicating $\lim_{g\to 0} f_i = 1$.

To summarise this section then, if the adiabatic approximation is good on the boundary of the vacuum valley, one can define a vacuum-valley wave function there, and easily derive its boundary conditions. The same adiabatic approximation allows one to then deduce the boundary condition eq. (4.15) on the wave function for Lüscher's effective hamiltonian. Moreover, if the coupling with the non-zero momentum modes (which were integrated out in Lüscher's effective hamiltonian) can be ignored, we argued that continuity of the energy density already implies the same boundary condition. In sect. 7 we will show that the adiabatic approximation at the boundary is good. This would allow a restriction to the vacuum-valley but implies furthermore that the coupling to the non-zero momentum modes can be

safely ignored. Consequently, we believe that our choice of boundary conditions gives an accurate description of the dynamics and that the agreement we found [6] with the Monte Carlo data in intermediate volumes is not a "numerical accident."

5. The Rayleigh-Ritz analysis

In this section we describe our basis for the Rayleigh-Ritz analysis and the implementation of gauge invariance. We then discuss Temple's inequality, which allows us to calculate rigorous upper *and* lower bounds for the energies once the hamiltonian is given. We also discuss projection onto the irreducible representations of the cubic group.

Because of the similarity to a three-particle quantum mechanics problem in a sphere, we construct a basis out of spherical harmonics $Y_{lm}(\theta, \phi)$ and radial eigenfunctions $\chi_{nl}(r)$ with radial quantum number n. At this point we only specify the boundary condition for $\chi_{nl}(r)$, which follows from (4.15):

$$\left(\frac{\mathrm{d}}{\mathrm{d}r}\right)^{(1-e_i)}(r\chi_{nl}(r))\Big|_{r=\pi} = 0. \tag{5.1}$$

The specific choices of $\chi_{nl}(r)$ are discussed later.

The question of imposing gauge invariance is completely independent of the radial eigenfunctions, because in our coordinates a gauge transformation is simply a rotation of the particle states. Thus imposing gauge invariance is equivalent to requiring that the three-particle states be singlets under SO(3):

$$\boldsymbol{L}_1 + \boldsymbol{L}_2 + \boldsymbol{L}_3 = \boldsymbol{0}. \tag{5.2}$$

Let $\langle \theta, \phi | l, m \rangle = Y_{lm}(\theta, \phi)$ and combine the first two "particles" into angular momentum eigenstates $|l_1 l_2 j, m\rangle$:

$$|l_1 l_2 j, m\rangle = \sum_{m_1, m_2} |l_1 l_2 m_1 m_2\rangle \langle l_1 l_2 m_1 m_2 | l_1 l_2 j, m\rangle, \tag{5.3}$$

where $|l_1 l_2 m_1 m_2\rangle \equiv |l_1 m_1\rangle |l_2 m_2\rangle$ and $\langle l_1 l_2 m_1 m_2 | l_1 l_2 j, m\rangle$ is a Clebsch-Gordan-Wigner coefficient, found in standard quantum mechanics texts. Here we just remind the reader that $\langle l_1 l_2 m_1 m_2 | l_1 l_2 j, m\rangle$ vanishes unless $m_1 + m_2 = m$ and $|l_1 - l_2| \leqslant j \leqslant l_1 + l_2$. Finally, we combine $|l_1 l_2 j, m\rangle$ and $|l_3 m_3\rangle$ into an SO(3) singlet, which requires $m_3 = -m$ and $l_3 = j$. Thus a triplet (l_1, l_2, l_3) uniquely labels a three-particle SO(3) singlet state, which we write as $|l_1 l_2 l_3\rangle$. Explicitly:

$$|l_1 l_2 l_3\rangle = \sum_{m_1, m_2, m_3} W(l_1 l_2 l_3 m_1 m_2 m_3) |l_1 m_1\rangle |l_2 m_2\rangle |l_3 m_3\rangle, \tag{5.4}$$

where

$$W(l_1 l_2 l_3 m_1 m_2 m_3)$$

$$= \delta_{m_1+m_2+m_3,0}(-1)^{l_3+m_3}\sqrt{\frac{(l_1+l_2-l_3)!(l_1+l_3-l_2)!(l_2+l_3-l_1)!}{(l_1+l_2+l_3+1)!}}$$

$$\times \sum_k \left\{ \frac{(-1)^k \sqrt{(l_1+m_1)!(l_1-m_1)!(l_2+m_2)!(l_2-m_2)!(l_3+m_3)!(l_3-m_3)!}}{k!(l_3-l_1-m_2+k)!(l_1+l_2-l_3-k)!(l_1-m_1-k)!(l_2+m_2-k)!} \right.$$

$$\left. \times \frac{1}{(l_3-l_2+m_1+k)!} \right\}. \quad (5.5)$$

Factorial arguments cannot be negative, so the range of the k sum is determined and constraints on the triplet (l_1, l_2, l_3) appear:

$$l_1 + l_2 \geqslant l_3, \qquad l_2 + l_3 \geqslant l_1, \qquad l_3 + l_1 \geqslant l_2. \quad (5.6)$$

This is equivalent to $|l_1 - l_2| \leqslant l_3 \leqslant l_1 + l_2$, (see above), but shows the permutation symmetry between the particles more explicitly. The Wigner coefficients W are also symmetric:

$$W(l_{\pi(1)} l_{\pi(2)} l_{\pi(3)} m_{\pi(1)} m_{\pi(2)} m_{\pi(3)}) = (-1)^{sg(\pi)(l_1+l_2+l_3)} W(l_1 l_2 l_3 m_1 m_2 m_3) \quad (5.7)$$

for any 3-permutation π.

To summarize, our *complete*, *gauge invariant* Rayleigh-Ritz basis consists of states $|l_1 l_2 l_3 n_1 n_2 n_3; e\rangle$ with

$$\langle c | l_1 l_2 l_3 n_1 n_2 n_3; e\rangle = \left(\prod_{i=1}^{3} \left(\chi^{(e_i)}_{n_i l_i}(r) \langle \theta_i, \phi_i | \right) \right) | l_1 l_2 l_3 \rangle$$

$$= \sum_{m_1, m_2, m_3} W(l_1 l_2 l_3 m_1 m_2 m_3) \prod_{i=1}^{3} \chi^{(e_i)}_{n_i l_i}(r) Y_{l_i m_i}(\theta_i, \phi_i),$$

$$n_i, l_i \in 0, 1, 2, \ldots, \qquad |l_1 - l_2| \leqslant l_3 \leqslant l_1 + l_2. \quad (5.8)$$

The electric flux quantum numbers $e_i \in Z_2$ appear from the boundary conditions on the 1-particle radial eigenfunctions (5.1). In practice, we always pick χ so that the basis vectors are eigenstates of some simple operator, say $-\frac{1}{2}\partial^2/(\partial c_i^a)^2$, with eigenvalues $\varepsilon(l_1 l_2 l_3 n_1 n_2 n_3)$.

Despite the constraint on l_i (eq. (5.6)), we have a large set of quantum numbers, and one might fear one needs too many basis vectors to get an accurate variational

state. It is thus helpful to project onto the irreducible representations of the symmetry group of our effective hamiltonian, which for $\boldsymbol{e}=\mathbf{0}$ or $\boldsymbol{e}=(1,1,1)$ is the full cubic group $O(3,Z)$. This acts on the i index of c_i^a and thus mixes the "particles". The projection also removes degeneracies caused by irreducible representations with dimension higher than 1. The cubic group has ten irreps:

$$A_1^p(1),\ A_2^p(1),\ E^p(2),\ T_1^p(3),\ T_2^p(3), \tag{5.9}$$

where $p=\pm 1$ is the eigenvalue for the parity operator P ($Pc_i^a=-c_i^a$), and the number in brackets is the irrep dimension. We construct these representations by noting the cubic group is the semidirect product of the coordinate permutations S_3 and the three Z_2 coordinate reflections P_i ($P_i c_k^a=-c_k^a(i=k),\ +c_k^a(i\neq k)$):

$$O(3,Z)=Z_2^3\rtimes S_3\,. \tag{5.10}$$

If $p_i=\pm 1$ is the eigenvalue of P_i we obviously have

$$\begin{aligned} p&=p_1p_2p_3\,,\\ P_i|l_1l_2l_3\rangle&=(-1)^{l_i}|l_1l_2l_3\rangle\,,\\ \pi|l_1l_2l_3n_1n_2n_3\rangle&=|l_{\pi(1)}l_{\pi(2)}l_{\pi(3)}n_{\pi(1)}n_{\pi(2)}n_{\pi(3)}\rangle\,, \end{aligned} \tag{5.11}$$

where $\pi\in S_3$ is a three-permutation acting on the particle index. The projection on the various representations can now be specified in terms of the triplets (q_1,q_2,q_3), where q stands for the pair of quantum numbers (l,n), i.e.,

$$|q_1q_2q_3\rangle\equiv|l_1l_2l_3n_1n_2n_3\rangle\,, \tag{5.12}$$

and we define an ordering

$$\begin{aligned} q<q'&\Leftrightarrow(l<l' \text{ or if } l=l', \text{ then } n<n')\,,\\ q=q'&\Leftrightarrow(l=l' \text{ and } n=n')\,. \end{aligned} \tag{5.13}$$

These projections are given in table 2. They are mutually orthogonal and block diagonalise the hamiltonian.

For electric flux $\boldsymbol{e}\neq\mathbf{0}$, $\boldsymbol{e}\neq(1,1,1)$ the cubic group is broken to $Z_2\times O(2,Z)=Z_2\times(Z_2^2\rtimes S_2)$, where S_2 permutes the directions with equal electric flux. In this work we only consider states that have positive parity p_i and are even under S_2. Such states are denoted e_N^+, where e_1^+ and e_2^+ are triplets with one and two units of electric flux respectively. We also write e_3^+ for the singlet with three units of electric flux, $\boldsymbol{e}=(1,1,1)$.

TABLE 2
Projection of the basis onto the irreducible representations

$$|q_1q_2q_3;\, A_1^p\rangle = \frac{N_q}{\sqrt{6}} \sum_{\pi\in S_3} |q_{\pi(1)}q_{\pi(2)}q_{\pi(3)}\rangle\,,$$
$$q_1 \geqslant q_2 \geqslant q_3\,, \qquad (-1)^{l_i} = p\,, \qquad \boldsymbol{e} = \mathbf{0};$$

$$|q_1q_2q_3;\, A_2^p\rangle = \frac{1}{\sqrt{6}} \sum_{\pi\in S_3} \operatorname{sg}\pi\, |q_{\pi(1)}q_{\pi(2)}q_{\pi(3)}\rangle\,,$$
$$q_1 > q_2 > q_3\,, \qquad (-1)^{l_i} = p\,, \qquad \boldsymbol{e} = \mathbf{0};$$

$$|q_1q_2q_3;\, E^p\rangle = N_q\Big(\frac{1}{\sqrt{3}}|q_1q_2q_3\rangle - \tfrac{1}{2}|q_1q_3q_2\rangle + \tfrac{1}{2}|q_3q_2q_1\rangle$$
$$- \frac{1}{2\sqrt{3}}|q_2q_3q_1\rangle - \frac{1}{2\sqrt{3}}|q_3q_1q_2\rangle\Big)\,,$$
$$q_1 > q_3,\ q_2 \geqslant q_3\,, \qquad (-1)^{l_i} = p\,, \qquad \boldsymbol{e} = \mathbf{0};$$

$$|q_1q_2q_3;\, T_1^p\rangle = \sqrt{\tfrac{1}{2}}\,(|q_1q_2q_3\rangle - |q_2q_1q_3\rangle);$$
$$q_1 > q_2\,, \qquad (-1)^{l_1+1} = (-1)^{l_2+1} = (-1)^{l_3} = p\,, \qquad \boldsymbol{e} = \mathbf{0};$$

$$|q_1q_2q_3;\, T_2^p\rangle = \sqrt{\tfrac{1}{2}}\,N_q(|q_1q_2q_3\rangle + |q_2q_1q_3\rangle);$$
$$q_1 \geqslant q_2\,, \qquad (-1)^{l_1+1} = (-1)^{l_2+1} = (-1)^{l_3} = p\,, \qquad \boldsymbol{e} = \mathbf{0};$$

$$|q_1q_2q_3;\, e_1^p\rangle = \sqrt{\tfrac{1}{2}}\,N_q(|q_1q_2q_3\rangle + |q_2q_1q_3\rangle);$$
$$q_1 \geqslant q_2\,, \qquad (-1)^{l_i} = p\,, \qquad \boldsymbol{e} = (0,0,1);$$

$$|q_1q_2q_3;\, e_2^p\rangle = \sqrt{\tfrac{1}{2}}\,N_q(|q_1q_2q_3\rangle + |q_2q_1q_3\rangle);$$
$$q_1 \geqslant q_2\,, \qquad (-1)^{l_i} = p\,, \qquad \boldsymbol{e} = (1,1,0);$$

$$|q_1q_2q_3;\, e_3^p\rangle = \sqrt{\tfrac{1}{6}}\,N_q \sum_{\pi\in S_3} |q_{\pi(1)}q_{\pi(2)}q_{\pi(3)}\rangle\,,$$
$$q_1 \geqslant q_2 \geqslant q_3\,, \qquad (-1)^{l_i} = p\,, \qquad \boldsymbol{e} = (1,1,1).$$

For each, only one element of the O(3, Z) orbit is given. N_q is a normalisation factor different from 1 if some q_i's are equal.

Thus the A_1^+ ground state, which is 8-fold degenerate for $g \to 0$, splits into two singlets A_1^+ and e_3^+ and two triplets e_1^+ and e_2^+ at larger g where electric flux energies are significant.

Following the prescriptions in table 2, we can build a separate basis for each type of representation, and diagonalise the hamiltonian separately in each sector.

The Rayleigh-Ritz procedure consists of simply truncating the infinite basis, to M vectors say. Diagonalising the truncated hamiltonian matrix provides a rigorous upper bound on each of the energy states [18]. The ordering of the basis is important, since we want an accurate approximation to the wave function. The

vectors were thus ordered by first truncating to $l_1 + l_2 + l_3 \leqslant L$ and $n_1 + n_2 + n_3 \leqslant N$. Then we ordered the basis vectors with increasing $\varepsilon(l_1 l_2 l_3 n_1 n_2 n_3)$, the sum of the one-particle energies (see later). Finally, we truncated this ordered basis to M vectors. This procedure more or less guarantees that the most important basis vectors are used, as we could verify by inspecting the coefficients of the eigenvectors.

However, to be completely sure no important basis vectors were omitted, we also used Temple's inequality to obtain a rigorous lower bound on the energy [18]. Suppose E_i is a discrete eigenvalue of a hamiltonian H, i.e., there exist eigenvalues E_{i-1} and E_{i+1} such that E_i is the only eigenvalue in the open interval (E_{i-1}, E_{i+1}). Suppose Ψ_i is the variational state for this eigenvalue (the ith eigenvector of the truncated hamiltonian), and is "reasonably good", i.e., $\langle \Psi_i | H | \Psi_i \rangle$ is smaller than E_{i+1}. Then one has for E_i the lower bound:

$$E_i \geqslant \langle \Psi_i | H | \Psi_i \rangle - T(K_i),$$

$$T(K_i) \equiv \frac{\langle \Psi_i | H^2 | \Psi_i \rangle - \langle \Psi_i | H | \Psi_i \rangle^2}{K_i - \langle \Psi_i | H | \Psi_i \rangle} \tag{5.14}$$

for any K_i in the half open interval $(\langle \Psi_i | H | \Psi_i \rangle, E_{i+1}]$. The sharpest bound is obviously obtained for $K_i = E_{i+1}$ (and is the best we can do, because it saturates for Ψ_i an arbitrary linear combination of the exact ith and $(i+1)$th eigenvectors). Since E_{i+1} is not known exactly, we use a conservative estimate

$$K_i = \tfrac{1}{2}(\langle \Psi_i | H | \Psi_i \rangle + \langle \Psi_{i+1} | H | \Psi_{i+1} \rangle). \tag{5.15}$$

Note that if $\langle \Psi_{i+1} | H | \Psi_{i+1} \rangle$ is close to E_{i+1} then $T(K_i) \simeq 2T(E_{i+1})$. We will list the Rayleigh-Ritz energies as $E_i = \langle \Psi_i | H | \Psi_i \rangle (\frac{1}{2} T(K_i))$, i.e., if we quote $E_i = a(b)$ this means $a - 2b \leqslant E_i \leqslant a$ is a rigorous bound, while $a - b \leqslant E_i \leqslant a$ is a safe bound. In practice we observed by varying M that E_i is far closer to its upper bound than to its lower bound.

The proof [18] of (5.14) follows from Temple's operator inequality $(H - E_i)(H - K) \geqslant 0$ for any $K \in [E_i, E_{i+1}]$. Note that to compute the lower bound we need the matrix for H^2.

We now discuss the radial wave functions $\chi_{nl}(r)$, chosen to be eigenfunctions of some convenient radial wave equation:

$$\left(-\frac{1}{2r^2} \frac{\mathrm{d}}{\mathrm{d}r} r^2 \frac{\mathrm{d}}{\mathrm{d}r} + \frac{l(l+1)}{2r^2} + V(r) \right) \chi_{nl}(r) = \varepsilon_{nl} \chi_{nl}(r), \tag{5.16}$$

together with the boundary condition (5.1). The hamiltonian in this basis is

$$\begin{aligned}
&\langle l_1 l_2 l_3 n_1 n_2 n_3 | H_{\text{eff}} | l_1' l_2' l_3' n_1' n_2' n_3' \rangle \\
&\quad = L^{-1} \left(\frac{1}{g^2} + \alpha_1 \right)^{-1} (\varepsilon_{n_1 l_1} + \varepsilon_{n_2 l_2} + \varepsilon_{n_3 l_3}) \, \delta_{n_1 n_1'} \delta_{l_1 l_1'} \delta_{n_2 n_2'} \delta_{l_2 l_2'} \delta_{n_3 n_3'} \delta_{l_3 l_3'} \\
&\qquad + \langle l_1 l_2 l_3 n_1 n_2 n_3 | V_{\text{T}}(c) | l_1' l_2' l_3' n_1' n_2' n_3' \rangle \\
&\qquad + \langle l_1 l_2 l_3 n_1 n_2 n_3 | V_l(c) - \left(\frac{1}{g^2} + \alpha_1 \right)^{-1} \sum_i V(r_i) | l_1' l_2' l_3' n_1' n_2' n_3' \rangle ,
\end{aligned} \tag{5.17}$$

with a similar expression for the matrix of H_{eff}^2, required for computing the lower bound.

To reduce to 1-particle matrix elements we first expand $V_l(c)$ in powers of r_i. Although $V_l(c)$ is known to infinite order (see eq. (2.22) and eq. (2.26)), we found it sufficient to expand to sixth order. To one loop, this can be read off from (2.16). We also added an eighth-order term to check stability; its coefficients were chosen to minimise the maximum error in V_l on $\boldsymbol{C} \in [0, \pi]^3$ to 0.3%. The expression we use for $V_l(c)$ is therefore:

$$\begin{aligned}
L \cdot V_l(c) \simeq\ & \gamma_1(g) \sum_i r_i^2 + \gamma_2(g) \sum_i r_i^4 + \gamma_3(g) \sum_{i>j} r_i^2 r_j^2 \\
& + \gamma_4(g) \sum_i r_i^6 + \gamma_5(g) \sum_{i \neq j} r_i^4 r_j^2 + \gamma_6(g) r_1^2 r_2^2 r_3^2 + \gamma_7(g) \sum_i r_i^8 \\
& + \gamma_8(g) \sum_{i \neq j} r_i^6 r_j^2 + \gamma_9(g) \sum_{i>j} r_i^4 r_j^4 + \gamma_{10}(g) \sum_i r_i^2 \left(r_1^2 r_2^2 r_3^2 \right) .
\end{aligned} \tag{5.18}$$

The functions $\gamma_N(g)$ accurate to two loops are listed in table 3, and we observe that the g dependence is surprisingly weak.

To keep track of the different types of approximations we have made, we will divide our results into three sets:

Type I ("Minimal hamiltonian"). These comprise the majority of our results. We neglect the sixth order part of V_{T}, all two-loop effects, and the eighth and higher order terms in V_l. This is the simplest approximation we can expect to give reasonable results, and amounts to putting $\alpha_3 = \alpha_4 = \alpha_5 = 0$ ($\kappa_8 = \kappa_9 = \kappa_{10} = 0$), $\gamma_7 = \gamma_8 = \gamma_9 = \gamma_{10} = 0$, and taking $\gamma_i(g) = \gamma_i(0)$ for $i < 7$.

Type II ("Full hamiltonian"). Here all displayed terms are included (except for a negligible 8th order two-loop contribution). We did some calculations to investigate the relative contributions of the 8th order one-loop, the two-loop, and the sixth order transverse terms. It turns out all 8th order terms can be ignored, while the other two are of roughly the same magnitude.

TABLE 3
Coefficients to two loops for the vacuum-valley effective potential V_l (eq. (5.18))

$$\begin{aligned}
\gamma_1(g) &= -0.30104661 \qquad\quad -0.30104661\,(g/2\pi)^2 \\
\gamma_2(g) &= -1.4488847\times10^{-3} - 9.9096768\times10^{-3}\,(g/2\pi)^2 \\
\gamma_3(g) &= 1.2790086\times10^{-2} + 3.6765224\times10^{-2}\,(g/2\pi)^2 \\
\gamma_4(g) &= 4.9676959\times10^{-5} + 5.2925358\times10^{-5}\,(g/2\pi)^2 \\
\gamma_5(g) &= -5.5172502\times10^{-5} + 1.8496841\times10^{-4}\,(g/2\pi)^2 \\
\gamma_6(g) &= -1.2423581\times10^{-3} - 5.7110724\times10^{-3}\,(g/2\pi)^2 \\
\gamma_7(g) &= -9.8738947\times10^{-7} - 5.1311245\times10^{-6}\,(g/2\pi)^2 \\
\gamma_8(g) &= 9.1911536\times10^{-6} + 9.1452409\times10^{-5}\,(g/2\pi)^2 \\
\gamma_9(g) &= -2.7911565\times10^{-5} - 2.5203366\times10^{-5}\,(g/2\pi)^2 \\
\gamma_{10}(g) &= 1.8208802\times10^{-5} + 6.0939067\times10^{-5}\,(g/2\pi)^2
\end{aligned}$$

Type III ("Truncated hamiltonian"). We set all coefficients α_i, κ_i and γ_i to zero. Although the results are not physical, the simplification allows a number of consistency checks and resolves an issue concerning the meaning of the T_1 and A_2 representations at weak coupling.

Lower bounds on the energies are only calculated for types I and III, because the full hamiltonian is too complicated to square easily.

Now we discuss the actual evaluation of the matrix elements, beginning with the angular parts. Here, three types of terms are involved ($\hat{c}_i^a = c_i^a/r_i$):

$$(i) \qquad \langle l_1 l_2 l_3 | \left(\hat{c}_i^a \hat{c}_j^a\right)^2 | l_1' l_2' l_3' \rangle \qquad (i \neq j),$$

$$(ii) \qquad \langle l_1 l_2 l_3 | \left(\hat{c}_i^a \hat{c}_j^a\right)^2 \left(\hat{c}_i^a \hat{c}_k^a\right)^2 | l_1' l_2' l_3' \rangle \qquad (i \neq j \neq k),$$

$$(iii) \qquad \langle l_1 l_2 l_3 | (\det \hat{c})^2 | l_1' l_2' l_3' \rangle .$$

These can all be calculated exactly, using (5.4), (5.5) and simple properties of spherical harmonics. The numerous symmetries imply we need (i) and (ii) for only a few values of i, j and k.

We are thus left with the radial reduced matrix elements, all of the form

$$F_e(n, n', l, i, j) \equiv \int_0^\pi \mathrm{d}r\, r^{2+2i+2j} \chi_{n,l}^{(e)}(r) \chi_{n',l+2j}^{(e)}(r). \tag{5.19}$$

The integers i and j are small,

$$\begin{aligned}
&j = 2, \quad i = 0 \qquad (\Delta l = 4), \\
&j = 1, \quad 0 \leqslant i \leqslant 3 \qquad (\Delta l = 2), \\
&j = 0, \quad 0 \leqslant i \leqslant 6 \qquad (\Delta l = 0).
\end{aligned} \tag{5.20}$$

For normalised eigenfunctions clearly $F_e(n, n', l, 0, 0) = \delta_{n,n'}$, but we will list the eigenfunctions without normalisation.

At this point we must finally be more specific about the radial 1-particle eigenfunctions χ, which are determined by the 1-particle potential $V(r)$ in (5.16), and the boundary conditions. We list three different choices A–C.

Type A ("Plane wave"). These are the spherical Bessel functions, i.e., spherical plane waves,

$$\chi_{nl}^{(e)}(r) = j_l\big(k_{nl}^{(e)} r\big),$$

$$V(r) = 0,$$

$$\varepsilon_{nl} = \tfrac{1}{2}\big(k_{nl}^{(e)}\big)^2, \tag{5.21}$$

which satisfy the boundary conditions (5.1). The boundary conditions determine the "momenta" $k_{nl}^{(e)}$:

$$j_l\big(k_{nl}^{(1)}\pi\big) = 0, \qquad \frac{\mathrm{d}}{\mathrm{d}z}\big(z j_l(z)\big)\Big|_{z = k_{nl}^{(0)}\pi} = 0. \tag{5.22}$$

The matrix elements $F_e(n, n', l, i, j)$ were calculated exactly in terms of $k_{nl}^{(e)}$, which were evaluated to 16-digit precision. This is elaborated upon in appendix C.

Type B ("Harmonic oscillator"). These are harmonic oscillator wave functions which because of the boundary conditions (5.1) have no simple ω-dependence:

$$\chi_{nl}^{(e)}(r) = r^l \mathrm{e}^{-\omega r^2/2} M\big(\tfrac{1}{2}l + \tfrac{3}{4} - \varepsilon_{nl}^{(e)}/(2\omega), l + \tfrac{3}{2}, \omega r^2\big),$$

$$V(r) = \tfrac{1}{2}\omega^2 r^2, \tag{5.23}$$

where $M(a, b; z)$ is a confluent hypergeometric or Kummer function, regular at $z = 0$ [19]. The 1-particle energies were evaluated numerically from the implicit definitions

$$M\big(\tfrac{1}{2}l + \tfrac{3}{4} - \varepsilon_{nl}^{(1)}/(2\omega), l + \tfrac{3}{2}, \omega r^2\big) = 0$$

$$(l + 1 - \omega\pi^2 - 2a) M\big(a, l + \tfrac{3}{2}, \omega\pi^2\big) + 2aM\big(a + 1, l + \tfrac{3}{2}, w\pi^2\big) = 0,$$

$$\varepsilon_{nl}^{(0)} = \omega\big(l + \tfrac{3}{2} - 2a\big). \tag{5.24}$$

The matrix elements $F_e(n, n', l, i, j)$ were calculated using 24- to 96-point gaussian integrations. Both ε and F_e depend in a complicated way on ω and have to be evaluated anew for each ω.

Type C ("Perturbative"). Here we take harmonic oscillator eigenfunctions, and impose no boundary conditions, demanding square integrability instead. These do

not distinguish between the different electrix fluxes, and are used to compare with the perturbative results of Lüscher and Münster [3]. This is partly for debugging and partly to investigate the spin content of the T_1 and A_2 representations at weak coupling. Thus we take

$$\chi_{nl}(r) = r^l e^{\omega r^2/2} L_n^{l+\frac{1}{2}}(\omega r^2),$$

$$V(r) = \tfrac{1}{2}\omega^2 r^2,$$

$$\varepsilon_{nl} = \omega\left(2n + l + \tfrac{3}{2}\right), \tag{5.25}$$

where $L_n^{\alpha}(z)$ are generalised Laguerre polynomials [19, ch. 13]. One easily derives analytic expressions for the matrix elements.

Our results will be classified by their type, the most common being type IA (minimal hamiltonian with a plane wave basis). The spherical plane wave basis is a very good basis for larger g values, beause at larger g the wave function becomes less peaked near the origin; its Fourier transform (effectively the coefficients of the wave function in the plane wave basis) will therefore concentrate around low momenta. At weaker coupling the harmonic oscillator basis tends to be better, because ω is an extra variational parameter that can be adjusted. For $0.5 \leqslant g \leqslant 1.4$ we used $\omega = 1.5$ and $\omega = 1.7$. The improvement is significant, although we expect that being able to increase the maximum value of $l_1 + l_2 + l_3$ would be most effective. For g values where we have accurate results for both bases we have observed up to 5 digit agreement.

We end this section with a few words about the computer programme, which was written in the language C. The UNIX environment proved useful for our complicated data handling. Angular matrix elements and 1-particle momenta were calculated and stored in files, reducing the building of the matrix for H_{eff} or H_{eff}^2 to simple algebraic operations. We then used routines from the IMSL library to diagonalise the hamiltonian. We used double precision throughout, but have performed quadruple precision calculations to check numerical stability. The maximal parameters were $l_1 + l_2 + l_3 \leqslant L = 20$, $n_1 + n_2 + n_3 \leqslant N = 10$ and $M = 800$. For this case $4\frac{3}{4}$ hours of CPU time on a Ridge-32 are spent diagonalising H, and $1\frac{1}{4}$ hours spent calculating the lower bound. Building the hamiltonian matrix took $2\frac{3}{4}$ min. Most runs were done with $M = 500$, requiring 2 h to calculate upper and lower bounds. If one calculates only the first few eigenvalues (and no eigenvectors, required for the lower bound) $\frac{1}{2}$ h of CPU time is used. Finally, CPU time is roughly proportional to M^3. The calculation is thus a non-trivial computation. However, because of the many cross checks, excellent agreement with previous results of Lüscher and Münster [3] and with our earlier semiclassical prediction, and the convergence of upper and lower bounds for increasing M, we are very confident of the numerical accuracy.

6. Comparison with the semiclassical result

This section is dedicated to a detailed comparison of the Rayleigh-Ritz results with the semiclassical prediction. Because our numerical results are for g values where there could be appreciable unknown corrections to the semiclassical expression, our approach will be to show that the two calculations agree up to beautifully simple correction terms, which vanish as $g \to 0$.

We first recall our prediction for the energy of three units of electric flux [4, 5]:

$$\Delta E(1,1,1) = E_0(1,1,1) - E_0(0,0,0)$$

$$= L^{-1}(1+f_0(g))^{-1} \cdot 3 \cdot 2\lambda B^2 g^{5/3} \exp\left(\frac{-S+Tg^{2/3}\varepsilon}{g}\right), \quad (6.1)$$

where

$$f_0(0) = 0,$$

$$\lambda = 0.6997\ldots,$$

$$B = 0.2063\ldots,$$

$$S = 12.4637\ldots,$$

$$T = 3.9186\ldots,$$

$$\varepsilon = 4.116719735\ldots, \quad (6.2)$$

and where the perturbative correction $f_0(g)$ is at least of order $g^{1/3}$. Eq. (6.1) is the rigorous weak-coupling expansion for ΔE, but as we have pointed out before [5], it was derived using only the lowest order expression $E_0 = g^{2/3}\varepsilon/L$ for the perturbative energy in the exponential. The higher order terms in E_0 are $O(g^{4/3})$, and omitting them causes the leading $(1 + O(g^{1/3}))$ correction. Thus we can increase the accuracy and range of applicability of (6.1) by replacing $g^{2/3}\varepsilon/L$ by the true perturbative energy. One option is to use the high order expansion of Lüscher and Münster [3]:

$$E_0 L = 4.116719735 g^{2/3} - 1.174516027 g^{4/3} - 0.118933 g^2$$

$$-0.03148 g^{8/3} + O(g^{10/3}). \quad (6.3)$$

The other option is to note that within the semiclassical approximation (i.e., up to $O(\Delta E^2)$ corrections) the perturbative energy is midway between the energy of three units of electric flux and the energy of zero units of electric flux. In table 4 the two definitions are compared, and their difference (larger than our rigorous numerical error bounds) is entirely consistent with small $O(g^{10/3})$ and $O(\Delta E^2)$ corrections.

TABLE 4
Type I(A&B) Rayleigh-Ritz results for the ground-state energies (in units of $1/L$) with $e = \mathbf{0}$ and $e = (1,1,1)$

g	$E_0(0,0,0)$	$E_0(1,1,1)$	$f(g)$	$\bar{E}$	E_{LM}	ΔE
0.5	2.09420(−451)	2.09414(−197)		2.0941(−30)	2.09257	
0.55	2.19391(−253)	2.19398(−98)		2.1939(−17)	2.19186	$0.00007\binom{+253}{-98}$
0.6	2.28578(−188)	2.28621(−79)		2.2860(−13)	2.28329	$0.00043\binom{+488}{-79}$
0.65	2.37026(−205)	2.37166(−77)	$-0.5277\binom{+5772}{-2806}$	2.3709(−10)	2.36752	$0.00140\binom{+250}{-78}$
0.7	2.44756(−269)	2.45119(−77)	$-0.5470\binom{+1220}{-1928}$	2.4493(−17)	2.44507	$0.00363\binom{+269}{-77}$
0.8	2.58031(−562)	2.59621(−61)	$-0.5744\binom{+170}{-1112}$	2.5882(−31)	2.58194	$0.01590\binom{+562}{-61}$
0.9	2.68229(−966)	2.72917(−41)	$-0.5956\binom{+36}{-691}$	2.7057(−50)	2.69679	$0.04688\binom{+966}{-41}$
1.0	2.75241(−1387)	2.85796(−22)	$-0.6113\binom{+8}{-451}$	2.8051(−70)	2.79179	$0.10555\binom{+1387}{-22}$
1.1	2.79242(−1271)	2.98977(−10)	$-0.6217\binom{+2}{-229}$	2.8911(−64)	2.86861	$0.19735\binom{+1271}{-10}$
1.2	2.80665(−1108)	3.13086(−4)	$-0.6262\binom{+1}{-123}$	2.9687(−55)	2.92859	$0.32421\binom{+1108}{-4}$
1.3	2.80000(−612)	3.28663(−4)	$-0.6242\binom{+1}{-47}$	3.0433(−31)	2.97280	$0.48663\binom{+612}{-4}$
1.4	2.77661(−378)	3.46178(−3)	$-0.6153\binom{+1}{-21}$	3.1192(−11)	3.00212	$0.68517\binom{+378}{-3}$
1.6	2.6908	3.8854	−0.5741	3.2881	3.01893	1.1946
1.8	2.5652	4.4238	−0.4930	3.4945	2.98364	1.8586
2.0	2.4129	5.0847	−0.3538	3.7488	2.89967	2.6718
2.2	2.2513	5.8639	−0.1224	4.0576	2.76958	3.6126
2.4	2.1011	6.7498	+0.2621	4.4255	2.59534	4.6487
2.6	1.9807	7.7276	+0.9040	4.8542	2.37849	5.7469

The perturbative factor $f(g)$ is defined in eq. (6.4), while E_{LM} is given in eq. (6.3) and $\bar{E}$ is an abbreviation for $\frac{1}{2}(E_0(0,0,0) + E_0(1,1,1))$. Where no bounds are quoted they are (far) better than the last ones tabulated.

Thus, incorporating this improvement into our prediction, we find:

$$\begin{aligned}\Delta E(1,1,1) &= E_0(1,1,1) - E_0(0,0,0)\\ &= L^{-1}(1+f(g))^{-1}6\lambda B^2 g^{5/3}\\ &\quad\times\exp\left(\frac{-S+\frac{1}{2}LT(E_0(1,1,1)+E_0(0,0,0))}{g}\right),\end{aligned}\tag{6.4}$$

We have no prediction for $f(g)$, but from the way it was derived (i.e., using [7] the path decomposition expansion), we expect it to be determined by the transverse fluctuations along the tunneling path, which have a perturbative expansion in g. All the non-adiabatic behaviour, causing powers of $g^{2/3}$, should enter through the perturbative wave function contribution to ΔE, which we have already accounted for [7]. However, since tunneling is expected to become significant only at $g \sim 0.7$,

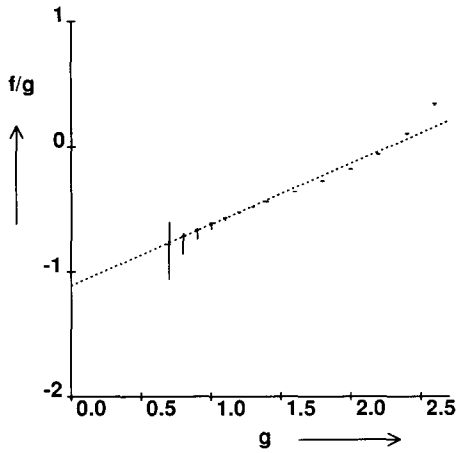

Fig. 3. The function $f(g)/g$ appearing in eq. (6.4) calculated using the Rayleigh-Ritz results for the minimal hamiltonian (type I(A&B)) to test the semiclassical result for the energy of electric flux.

where the exponent in eq. (6.1) changes sign, $f(g)$ is not guaranteed to be small in the region of interest, and could be ~ 1. This is why we should be careful in comparing Rayleigh-Ritz results with the semiclassical expression. The best we can do is confirm $f(g)$ is a simple power series in g, vanishing as $g \to 0$, with coefficients of order unity.

To test all this reasoning, note that for our favourite two-dimensional vacuum-valley toy model, where transverse fluctuations are exactly quadratic, we would expect $f(g)$ to be zero up to $O(\Delta E^2)$ corrections. Appendix B confirms this to high accuracy. There we provide the perturbative, semiclassical, Rayleigh-Ritz and Monte Carlo analyses performed on this toy model as a warm-up for the Yang-Mills case.

Table 4 gives our highest accuracy data (type IA&B) for $E_0(0,0,0)$ and $E_0(1,1,1)$, as well as the value of $f(g)$. Below $g = 0.7$ no reliable estimate is possible. In fig. 3 we plot $f(g)/g$ versus g and see remarkably near-linear behaviour over a wide range of g. To a good approximation

$$f(g) = -1.11g + 0.49g^2 \qquad \text{(dotted line)}. \tag{6.5}$$

However, the need to extrapolate from $g = 0.7$ to $g = 0$ does leave room for doubt, so we designed a rather sensitive test. We repeated both the semiclassical and the Rayleigh-Ritz analysis for the truncated hamiltonian (type III)

$$-\frac{g^2}{2}\frac{\partial^2}{(\partial c_i^a)^2} + \frac{1}{2g^2}\sum_{i>j}\left[c_i^a c_i^a c_j^b c_j^b - \left(c_i^a c_j^a\right)^2\right]. \tag{6.6}$$

In this case, the lowest order perturbative wave function and energy are exact, with no higher order corrections. Moreover, they are equal to the lowest order wave function and energy in the full problem. Thus

$$\Delta E' = L^{-1}(1+f'(g))^{-1}6\lambda' B^2 g^{5/3}\exp\left(\frac{-S'+T'g^{2/3}\varepsilon}{g}\right), \tag{6.7}$$

with B and ε the same as in eq. (6.1). However, S', T' and λ' are now determined by the simple 1-loop effective potential $2|C|$ ($|C_i| \leqslant \pi$), giving the (rescaled) double-cone problem solved in ref. [7]. So

$$S' = 2\int_0^\pi \mathrm{d}C\sqrt{2\cdot 2C} = \tfrac{8}{3}\pi^{3/2},$$

$$T' = 2\int_0^\pi \mathrm{d}C\frac{1}{\sqrt{2\cdot 2C}} = 2\pi^{1/2},$$

$$\lambda' = \frac{1}{(2\pi)^{1/2}}. \tag{6.8}$$

One calculates λ' as in ref. [7], sect. 4.

TABLE 5
Type III(A&B) Rayleigh-Ritz results for the ground-state energies (in units of $1/L$) with $e = \mathbf{0}$ and $e = (1,1,1)$

g	$E_0(0,0,0)$	$E_0(1,1,1)$	$f'(g)$	$\bar{E}$	$g^{2/3}\varepsilon$	ΔE
0.65	3.08974(−1218)	3.08911(−72)		3.08943(−645)	3.089064	
0.7	3.245459(−19)	3.245564(−12)	$2.1884(^{+4114}_{-4883})$	3.245512(−16)	3.245513	$0.000105(^{+19}_{-12})$
0.8	3.54724(−3)	3.54808(−1)	$2.4510(^{+411}_{-1190})$	3.54766(−2)	3.547682	$0.00084(^{+3}_{-1})$
0.9	3.83535(−8)	3.83941(−4)	$2.7290(^{+368}_{-723})$	3.83738(−6)	3.837482	$0.00406(^{+8}_{-4})$
1.0	4.10939(−24)	4.12310(−4)	$3.0625(^{+118}_{-711})$	4.11625(−14)	4.116720	$0.01371(^{+24}_{-4})$
1.1	4.36712(−75)	4.40369(−4)	$3.3509(^{+48}_{-892})$	4.38541(−40)	4.386786	$0.03657(^{+75}_{-4})$
1.2	4.60504(−18)	4.68621(−6)	$3.6364(^{+34}_{-103})$	4.64563(−12)	4.648778	$0.08117(^{+18}_{-6})$
1.3	4.81977(−29)	4.97615(−6)	$3.9325(^{+19}_{-91})$	4.89796(−18)	4.903583	$0.15638(^{+29}_{-6})$
1.4	5.00887(−43)	5.27902(−7)	$4.2459(^{+14}_{-83})$	5.14395(−25)	5.151930	$0.27015(^{+43}_{-7})$
1.5	5.17151(−65)	5.60011(−8)	$4.5912(^{+10}_{-85})$	5.38581(−37)	5.394429	$0.42860(^{+65}_{-8})$
1.6	5.30831(−84)	5.94422(−9)	$4.9907(^{+8}_{-79})$	5.62627(−47)	5.631593	$0.63591(^{+84}_{-9})$
1.7	5.42091(−103)	6.31550(−11)	$5.4695(^{+8}_{-74})$	5.86821(−57)	5.863864	$0.89459(^{+103}_{-11})$
1.8	5.51160(−121)	6.71734(−11)	$6.0592(^{+8}_{-71})$	6.11447(−66)	6.091622	$1.20574(^{+121}_{-11})$
1.9	5.58317(−137)	7.15231(−10)	$6.7983(^{+5}_{-68})$	6.36774(−74)	6.315199	$1.56914(^{+137}_{-10})$
2.0	5.63886(−150)	7.62228(−10)	$7.7380(^{+4}_{-66})$	6.63057(−80)	6.534885	$1.98342(^{+150}_{-10})$

The perturbative factors $f'(g)$ and ε are defined in eqs. (6.2) and (6.7), and $\bar{E}$ is $\frac{1}{2}(E_0(0,0,0)+E_0(1,1,1))$.

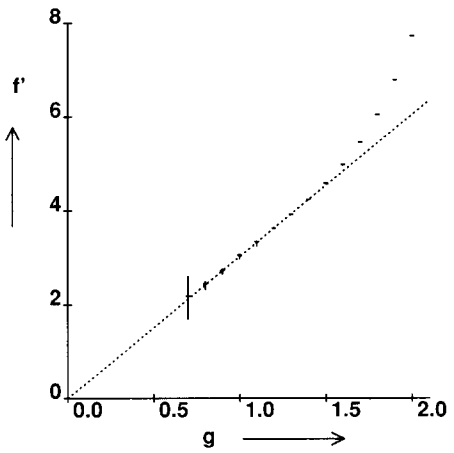

Fig. 4. The function $f'(g)$ appearing in eq. (6.7) calculated using the Rayleigh-Ritz results for the truncated hamiltonian (type III(A&B)) to test the semiclassical result for the energy of electric flux in the truncated model.

Numerical results (type IIIA&B) for this truncated model are in table 5, and in fig. 4 we plot $f'(g)$ versus g. We find

$$f'(g) = 3.03g \qquad \text{(dotted line)}, \tag{6.9}$$

again over a large range of g.

We regard eqs. (6.5) and (6.9) as excellent evidence for the consistency of the semiclassical and Rayleigh-Ritz analyses.

7. Nonadiabatic behaviour

In this section we analyse the deviation from adiabatic behaviour. We first describe the method of calculation, but most of this section presents and discusses numerical results. As described in sect. 3, the wave function can be decomposed into an infinite component vacuum-valley wave function by projection:

$$\Phi^{(i)}(C) = \int_{(S^2)^3} \prod_k (r_k \, d\Omega_k) \, \chi^{(i)}_{[C]}(\theta_k, \phi_k) \Psi(c) . \tag{7.1}$$

Here χ is the transverse eigenfunction satisfying

$$H_{tr} \chi^{(i)}_{[C]}(\theta_k, \phi_k) = V^{(i)}_{tr}(C) \chi^{(i)}_{[C]}(\theta_k, \phi_k) . \tag{7.2}$$

The transverse hamiltonian is given in eq. (3.5). We will perform the analysis only for the minimal (type I) and truncated (type III) hamiltonians. Thus for type I we have explicitly

$$L \cdot H_{\mathrm{tr}} = \left(\frac{1}{g^2} + \alpha_1\right)^{-1} \sum_i \frac{\boldsymbol{L}_i^2}{2r_i^2} + \frac{1}{2}\left(\frac{1}{g^2} + \alpha_2\right) \sum_{i>j} r_i^2 r_j^2$$

$$\times \left[1 - \sin^2\theta_i \sin^2\theta_j \left(\cos^2\phi_i \cos^2\phi_j + \sin^2\phi_i \sin^2\phi_j\right) - \cos^2\theta_i \cos^2\theta_j\right], \quad (7.3)$$

and for type III we put $\alpha_1 = \alpha_2 = 0$ in this equation. Obviously $V_{\mathrm{tr}}^{(i)}$ is found by diagonalising the matrix of H_{tr} in the basis $|l_1 l_2 l_3\rangle$. This requires only a minor change in our Rayleigh-Ritz programme: simply restrict n_i to zero and for the radial matrix elements use $F_e(0, 0, l, p, q) = r^{2(p+q)}$, i.e., freeze the r_i coordinates.

Clearly, when all r_i are unequal, there is no permutation symmetry and the cubic group is broken down to the coordinate reflections Z_2^3. Thus $\Phi^{(i)}$ in eq. (7.1) is only non-zero if the parities, $(-1)^{l_i}$, for $\chi_{[C]}^{(i)}$ are the same as for Ψ (see table 2). This has an important consequence: we expect transverse states involving odd parity to have higher transverse energy than those involving even parity. Thus wave functions Ψ involving odd parities see a higher quantum induced potential barrier, and tunneling sets in at higher values of g. This explains why, for the A_1^- state, the agreement between our Rayleigh-Ritz results and the perturbative expansion of Lüscher and Münster is good up to $g = 1.2$, where the difference is only 0.5%. Similarly, tunneling for the T_2 representation is expected to set in later than for the E representation, which we confirm in our variational analysis [6]. Sect. 8 gives some details.

Diagonalising the whole hamiltonian and the transverse hamiltonian gives

$$\Psi(c) = \lambda_{l_1 l_2 l_3 n_1 n_2 n_3} \langle c | l_1 l_2 l_3 n_1 n_2 n_3 \rangle,$$

$$\chi_{[C]}^{(i)}(\theta_k, \phi_k) = \mu_{l_1 l_2 l_3}^{(i)}(\boldsymbol{C}) \langle \theta_k, \phi_k | l_1 l_2 l_3 \rangle, \quad (7.4)$$

which provides a straightforward expression for $\Phi^{(i)}(\boldsymbol{C})$:

$$\Phi^{(i)}(\boldsymbol{C}) = \sum_{\{\boldsymbol{n}, \boldsymbol{l}\}} \left(\prod_{j=1}^{3} r_j \chi_{n_j l_j}(r_j)\right) \mu_{l_1 l_2 l_3}^{(i)}(\boldsymbol{C}) \lambda_{l_1 l_2 l_3 n_1 n_2 n_3}. \quad (7.5)$$

The only difficulty is that we have to "undo" the projections defined in table 2. We next computed the "non-adiabaticity fractions" f_i defined in eq. (4.16) by using 12×12-point gaussian integration for the two-dimensional integrals. We also calculated, for individual points $\boldsymbol{C}$, the fraction of the wave function in each component

of the vacuum-valley decomposition:

$$f_i^{(j)}(\boldsymbol{C}) = \frac{\Phi^{(j)}(\boldsymbol{C})^2}{\sum_{k=1}^{\infty} \Phi^{(k)}(\boldsymbol{C})^2}, \tag{7.6}$$

The denominator was calculated independently using

$$\sum_{k=1}^{\infty} \Phi^{(k)}(\boldsymbol{C})^2 = \sum_{\{\boldsymbol{n},\boldsymbol{l}\}} \left[\lambda_{l_1 l_2 l_3 n_1 n_2 n_3} \prod_{i=1}^{3} r_i \chi_{n_i l_i}(r_i) \right]^2, \tag{7.7}$$

to avoid calculating all transverse eigenfunctions $\chi_{[\boldsymbol{C}]}^{(j)}$. We do, however, confirm that $f_i^{(k)}$ decreases rapidly with k, and the sum of the first two or three pointwise fractions is very close to 1.

Note that $f_i^{(j)}(\boldsymbol{C})$ provides a different interpretation for f_i, being the weighted average of the pointwise fractions $f_i^{(1)}(\boldsymbol{C})$ over one face of the vacuum-valley boundary:

$$f_i = \lim_{r_i \to \pi} \int_0^{r_i} \int_0^{r_i} \mathrm{d}r_j \, \mathrm{d}r_k \, f_i^{(1)}(\boldsymbol{C}) w_i(\boldsymbol{C}), \tag{7.8}$$

where the weight $w_i(\boldsymbol{C})$ is proportional to the square of the wave function at $\boldsymbol{C}$:

$$w_i(\boldsymbol{C}) = \frac{1}{W_i(r_i)} \sum_{q=1}^{\infty} \Phi^{(q)}(\boldsymbol{C})^2,$$

$$W_i(r_i) = \int_0^{r_i} \int_0^{r_i} \mathrm{d}r_j \, \mathrm{d}r_k \sum_{q=1}^{\infty} \Phi^{(q)}(\boldsymbol{C})^2. \tag{7.9}$$

At first sight one might think the adiabatic approximation is only good if the pointwise fractions at the boundary $r_i = \pi$ are uniformly small. However, the following argument shows this is incorrect. Suppose the adiabatic assumption is exact, and let Ψ be the E^+ or T_1^+ state. For each of these, $\Phi^{(1)}(\boldsymbol{C})$ has a nodal surface, dictated by symmetry, which intersects the boundary $r_i = \pi$. Thus if we switch on some arbitrarily small non-adiabatic corrections, $f_i^{(1)}(\boldsymbol{C}) \equiv 0$ at the nodal surface. The adiabatic approximation is nevertheless good because the probability $w_i(\boldsymbol{C})$ of actually being at this point is arbitrarily small. Thus eq. (7.8) is the appropriate measure of the accuracy of the adiabatic approximation. However, as stated at the outset, we will not try to estimate the size of corrections as a function of $(1 - f_i)$. Such an analysis would have to include the effect of off-diagonal coupling illustrated in fig. 2, which as explained in sect. 4, could be *enhancing* the accuracy of our results at higher g. Unfortunately, we are lacking an expansion

TABLE 6
Adiabaticity parameter f_i, eq. (4.16) (upper number) and integral of the wave function squared W_i, eq. (7.9b) (lower number) for the states in column 1 and surfaces in column 2

		$g=1.0$	$g=1.5$	$g=2.0$	$g=2.6$
A_1^+	$r_3=\pi$	0.9607 5.590×10^{-2}	0.9482 2.387×10^{-1}	0.9173 3.767×10^{-1}	0.9284 5.095×10^{-1}
$(A_1^+)'$	$r_3=\pi$	0.9856 3.752×10^{-1}	0.9667 5.865×10^{-1}	0.9182 6.702×10^{-1}	0.8858 6.935×10^{-1}
A_1^-	$r_3=\pi$	0.8951 6.801×10^{-3}	0.8938 1.554×10^{-1}	0.8898 $4.167\cdot10^{-1}$	0.9709 $6.659\cdot10^{-1}$
E^+	$r_1=\pi$	0.9456 $1.026\cdot10^{-1}$	0.9407 $2.866\cdot10^{-1}$	0.9208 $4.404\cdot10^{-1}$	0.9522 $5.621\cdot10^{-1}$
	$r_2=\pi$	0.9586 $5.112\cdot10^{-1}$	0.9542 $5.969\cdot10^{-1}$	0.9583 $6.195\cdot10^{-1}$	0.9769 $6.331\cdot10^{-1}$
	$r_3=\pi$	0.9564 $3.069\cdot10^{-1}$	0.9498 $4.417\cdot10^{-1}$	0.9428 $5.299\cdot10^{-1}$	0.9653 $5.976\cdot10^{-1}$
T_1^+	$r_1=\pi$	0.9753 $7.571\cdot10^{-1}$	0.9740 $7.007\cdot10^{-1}$	0.9717 $4.669\cdot10^{-1}$	0.9277 $4.032\cdot10^{-1}$
	$r_3=\pi$	0.9797 $9.179\cdot10^{-2}$	0.9622 $3.101\cdot10^{-1}$	0.9202 $4.565\cdot10^{-1}$	0.8664 $5.671\cdot10^{-1}$
T_2^+	$r_1=\pi$	0.9789 $6.840\cdot10^{-1}$	0.9722 $6.456\cdot10^{-1}$	0.9670 $1.018\cdot10^{-0}$	0.9608 $8.114\cdot10^{-1}$
	$r_3=\pi$	0.9840 $7.463\cdot10^{-2}$	0.9739 $2.569\cdot10^{-1}$	0.9350 $3.716\cdot10^{-1}$	0.8953 $4.901\cdot10^{-1}$
e_1^+	$r_1=3$	0.9667 $6.340\cdot10^{-2}$	0.9530 $2.648\cdot10^{-1}$	0.9444 $5.627\cdot10^{-1}$	0.9730 $7.536\cdot10^{-1}$
	$r_3=3$	0.9353 $1.671\cdot10^{-3}$	0.8959 $4.135\cdot10^{-3}$	0.8650 $6.378\cdot10^{-3}$	0.9284 $8.571\cdot10^{-3}$
e_2^+	$r_1=3$	0.9310 $1.636\cdot10^{-3}$	0.8937 $4.841\cdot10^{-3}$	0.9144 $4.537\cdot10^{-3}$	0.9707 $5.258\cdot10^{-3}$
	$r_3=3$	0.9631 $6.245\cdot10^{-2}$	0.9472 $3.306\cdot10^{-1}$	0.9580 $5.271\cdot10^{-1}$	0.9874 $6.281\cdot10^{-1}$
e_3^+	$r_3=3$	0.9318 $1.855\cdot10^{-3}$	0.8972 $6.258\cdot10^{-3}$	0.9293 $1.011\cdot10^{-2}$	0.9808 $1.240\cdot10^{-2}$

Note $(A_1^+)'$ is the first excited A_1^+ state.

parameter for this type of analysis, but it just might explain why our variational results seem to agree better with the higher statistics Monte Carlo data of ref. [20] at $g\sim2.6$ than at $g\sim2$ (see ref. [6]). For more details we refer to sect. 8.

In table 6 we give our numerical results for the fractions f_i (eq. (4.16)). For practical reasons we compute f_i for non-zero electric flux at $r_i=3$, because the wave function is zero at $r_i=\pi$ if $e_i=1$. The table also gives the integral of the wave function squared (W_i) over a boundary face. We provide data for groundstates in the sectors A_1^+, A_1^-, E^+, T_1^+, T_2^+, e_1^+, e_2^+, e_3^+, and for the first excited A_1^+ state (which we call $(A_1^+)'$), for g values of 1.0, 1.5, 2.0 and 2.6. Symmetries (table 2) relate the f_i within each sector as follows: $f_1=f_2=f_3$ for A_1^+ and e_3^+, $f_1=f_2$ for T_1^+, T_2^+, e_1^+, e_2^+, whereas all f_i are different for E^+. The W_i are related similarly.

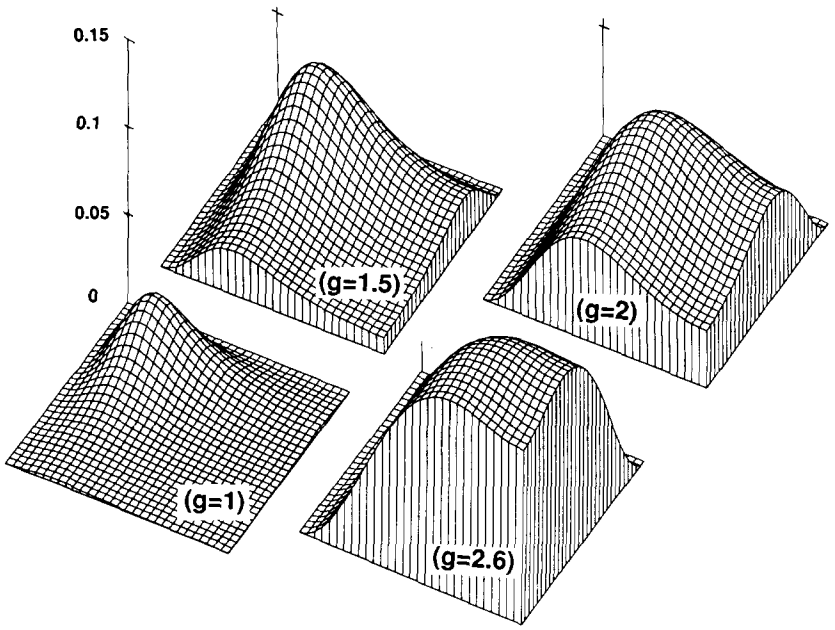

Fig. 5. Plots for the probability density of the A_1^+ ground-state wave function at $r_3 = \pi$ as a function of r_1 and r_2 on $[0, \pi]^2$. The vertical axis is positioned at (0,0) and the vertical scales are the same in each plot.

A number of interesting observations can be made through inspecting table 6. We see the effect illustrated in fig. 2 confirmed, since f_i *increases* beyond $g = 2$ for most states. The fraction of the wave function possibly leaking to the excited transverse sectors is always less than 15%, and usually much less. From this evidence, we expect that non-adiabatic corrections to our energy levels are no more than 5 to 10%.

From table 4 we also see that W_i increases with g. The suppression of tunneling at lower g is clearly visible in the A_1^- state, and to some extent in A_1^+, e_1^+, e_2^+ and e_3^+. It thus confirms that for A_1^- the tunneling sets in at larger g values (presumably $g \sim 1.2$), whereas for the other states tunneling has already set in at $g < 0.8$.

A third effect, which is quite dramatic, is illustrated in fig. 5. There we plot the probability density $\sum_q \Phi^{(q)}(C)^2$ over one face (say $r_3 = \pi$), for the groundstate A_1^+. The vertical scale is the same on each graph, and horizontally we plot r_1 and r_2 from 0 to π, with (0,0) at the vertical axis. We see that towards larger g the wave function tends to concentrate around $r_i = \pi$, rather than close to $r_i = 0$, which can be considered as the "Z_2-symmetry restoration". All other representations show similar effects (e.g., see fig. 6 and fig. 8).

From fig. 5 we also see the effect mentioned in sect. 3. At smaller g, the wave function peaks near to $r_i = 0$, and we conjecture that the maximum at fixed r_2, r_3 moves to $r_1 = 0$ as $g \to 0$, thereby effectively turning the vanishing boundary

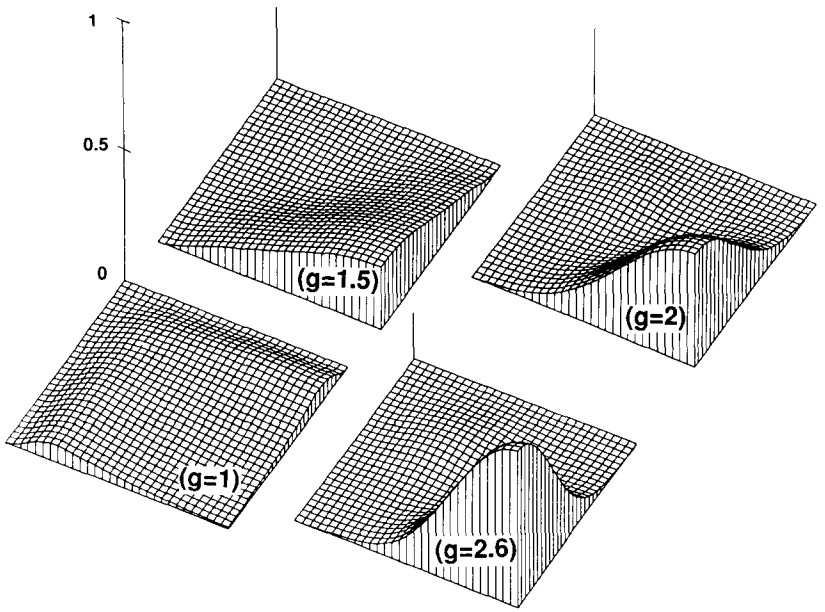

Fig. 6. Plots for the probability density of the first excited A_1^+ state at $r_3 = \pi$ as a function of r_1 and r_2 on $[0, \pi]^2$. The vertical axis is positioned at (0,0) and the vertical scales are the same in each plot.

condition on $\Phi^{(1)}$ at $r_i = 0$ into the condition $\partial\Phi^{(1)}/\partial r_i = 0$ at $r_i = 0$. All representations show a similar peaking.

In fig. 6 we give the probability density for $(A_1^+)'$, the first excited A_1^+ state. The new feature exhibited there is revealed more clearly in fig. 7, which gives for the non-adiabatic fraction $\frac{1}{3}(1 - f_3^{(1)}(\boldsymbol{C}))$ as a function of r_1 and r_2 for $r_3 = \pi$. Again vertical scales are the same for each g, and the vertical axis is drawn at $(r_1, r_2) = (0,0)$. What we see appearing at $g = 1.5$ is the nodal surface of $\Phi^{(1)}(\boldsymbol{C})$, which for small g is a sphere centered at $\boldsymbol{C} = 0$, with radius $O(g^{2/3})$. Only at large enough g is it expected to intersect with the boundary. As was explained earlier, at such a nodal surface f will become zero, and fig. 7 clearly illustrates this feature. The nodal surfaces are harder to see in fig. 6, but can still be made out.

Fig. 8 gives probability densities for the E^+ state at $g = 1$ and $g = 2$, for each of the faces $r_1 = \pi$ (a), $r_2 = \pi$ (b), $r_3 = \pi$ (c). Here the nodes are dictated by symmetry, and they persist down to $g = 0$, the nodal curve at $r_1 = \pi$ being particularly conspicuous. Although we do not present the graph, we have observed that these nodes coincide with highly isolated zero's in the fractions f_i, just as in fig. 7. We leave it to the reader to visualise how the three faces in fig. 8 combine into one continuous function.

We end this section with a discussion of the behaviour of $V_{\rm tr}^{(i)}$ and $\boldsymbol{A}_{km}$ to illustrate the point made at the end of sect. 3. This requires us to calculate the quantity $(\partial/\partial r_i)\chi_{[\boldsymbol{C}]}^{(j)}$. The problem is similar to one faced in appendix B, since it is

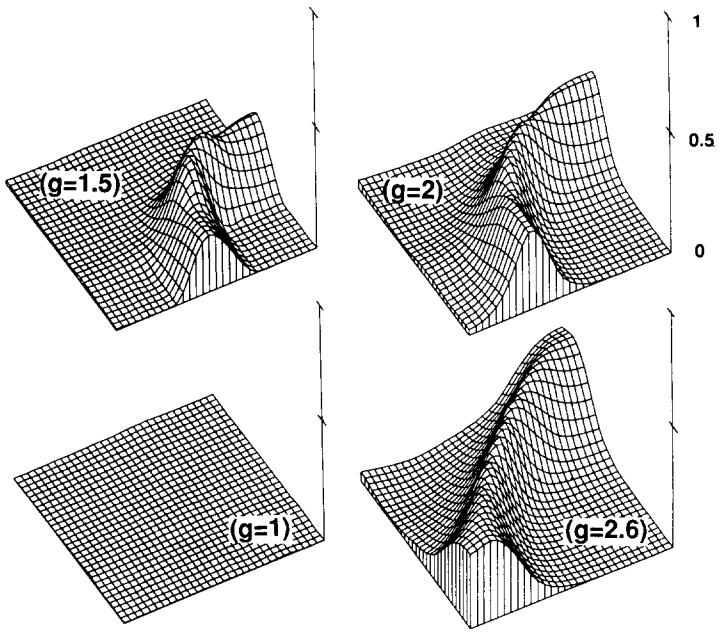

Fig. 7. Plots for the nonadiabatic fractions of the first excited A_1^+ state at $r_3 = \pi$ as a function of r_1 and r_2 on $[0, \pi]^2$. The vertical axis is positioned at (0,0) and the vertical scale, the same in each plot, gives $\frac{1}{3}(1 - f_3^{(1)}(\boldsymbol{C}))$. The "mountain range", for which $f_3^{(1)}(\boldsymbol{C}) = 0$, corresponds to the node in fig. 6.

equivalent to calculating the first order correction to the eigenvectors of the transverse hamiltonian $H_{\rm tr}(r_i + \varepsilon)$. One easily finds a linear equation determining $(\partial/\partial r_i)\chi_{[C]}^{(j)}$:

$$\left(H_{\rm tr} - V_{\rm tr}^{(j)}\right)\frac{\partial}{\partial r_i}\chi_{[C]}^{(j)} = -\left(\frac{\partial H_{\rm tr}}{\partial r_i} - \frac{\partial V_{\rm tr}^{(j)}}{\partial r_i}\right)\chi_{[C]}^{(j)}, \tag{7.10}$$

which can be converted to a *non-singular* matrix equation (by adding $\mu_l\mu_k$)

$$\left(H_{l,k} - V_{\rm tr}^{(j)}\delta_{l,k} + \mu_l\mu_k\right)\nu_k = \left(\mu_p(\Delta H)_{p,q}\mu_q\,\delta_{l,k} - (\Delta H)_{l,k}\right)\mu_k. \tag{7.11}$$

Here we have suppressed $\boldsymbol{C}$ dependence, and write

$$|\boldsymbol{l}\rangle = |l_1 l_2 l_3\rangle,$$

$$H_{l,k} = \langle \boldsymbol{l}|H_{\rm tr}|\boldsymbol{k}\rangle,$$

$$(\Delta H)_{l,k} = \langle \boldsymbol{l}|\frac{\partial H_{\rm tr}}{\partial r_i}|\boldsymbol{k}\rangle,$$

$$\chi_{[C]}^{(j)}(\theta_k, \phi_k) = \mu_l\langle\{\theta_k, \phi_k\}|\boldsymbol{l}\rangle,$$

$$\frac{\partial}{\partial r_i}\chi_{[C]}^{(j)}(\theta_k, \phi_k) = \nu_l\langle\{\theta_k, \phi_k\}|\boldsymbol{l}\rangle. \tag{7.12}$$

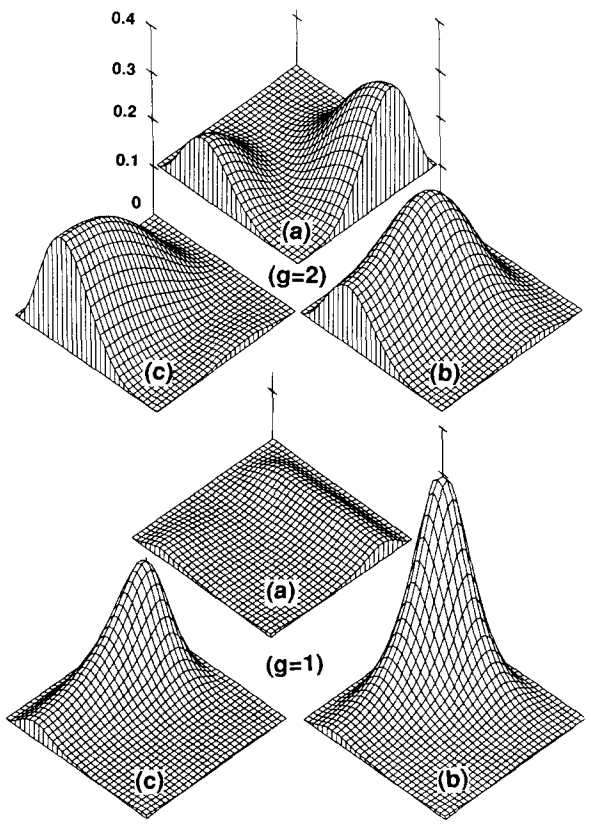

Fig. 8. Plots for the probability density of the E^+ ground-state wave function at (a) $r_1 = \pi$ as a function of r_2 and r_3 on $[0, \pi]^2$, (b) $r_2 = \pi$ as a function of r_1 and r_3 on $[0, \pi]^2$ and (c) $r_3 = \pi$ as a function of r_1 and r_2 on $[0, \pi]^2$. The vertical axis is positioned at (0,0) and the vertical scales are the same in each plot.

Consideration of eq. (7.12) shows that the matrix ΔH is a trivial variation on the matrix H, so one readily solves eq. (7.11) to obtain v_l. Note that $(\partial/\partial r_i)\chi^{(j)}_{[C]}$ is orthogonal to $\chi^{(j)}_{[C]}$ since the latter is normalised to 1.

We can now calculate $\boldsymbol{A}_{ij}$ as defined in eq. (3.8). A useful check is

$$\int_{(S^2)^3} \prod_i d\Omega_i \sum_k \left[\frac{\partial}{\partial r_k} \chi^{(j)}_{[C]}(\{\theta_m, \phi_m\}) \right]^2 = \sum_{i=1}^{\infty} \left[\boldsymbol{A}_{ij}(\boldsymbol{C}) \right]^2. \tag{7.13}$$

We observed that the sum over i is dominated by the first few non-zero terms.

Results for $g = 1.0$, type III, are given in figs. 10 and 11. The former shows $r_3 = 2$ and the latter $r_3 = 3$. Only the even parity sector is presented, and we plot (a): $\Sigma_k [\boldsymbol{A}_{k1}(\boldsymbol{C})]^2$, (b): $\Sigma_k [A^3_{k1}(\boldsymbol{C})]^2$, (c): $V^{(2)}_{\rm tr}(\boldsymbol{C}) - V^{(1)}_{\rm tr}(\boldsymbol{C})$ and (d): $V^{(1)}_{\rm tr}(\boldsymbol{C})$. These graphs clearly do show a region of intricate behaviour at intermediate values of r_1

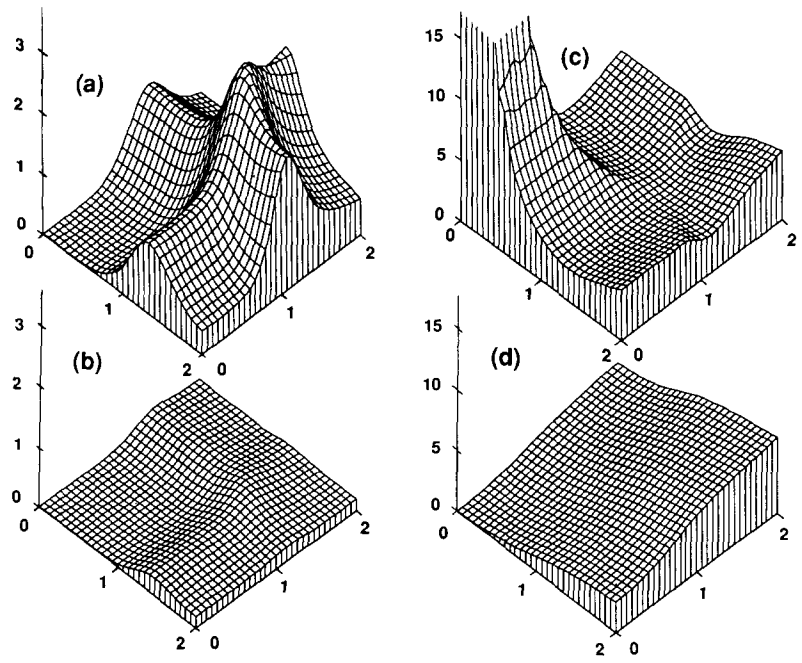

Fig. 9. Plots at $r_3 = 2$ as a function of r_1 and r_2 for (a) $(A_{k1}(C))^2$, (b) $(A^3_{k1}(C))^2$, (c) $L \cdot (V^{(2)}_{\rm tr}(C) - V^{(1)}_{\rm tr}(C))$ and (d) $L \cdot V^{(1)}_{\rm tr}(C)$.

and r_2, as discussed at the end of sect. 3. We have confirmed this intermediate region shifts towards $r_1 = 0$, $r_2 = 0$ as g decreases, and that $\Sigma_k [A^3_{k1}(C)]^2$ becomes negligible. As can be seen in the figures, the one-loop result holds for large enough C, where $V^{(1)}_{\rm tr}(C) = 2|C|$ and $V^{(2)}_{\rm tr}(C) = 4|C|$ (the transverse state with energy $3|C|$ has negative parity) so that $V^{(2)}_{\rm tr} - V^{(1)}_{\rm tr} = V^{(1)}_{\rm tr}$. We have also confirmed that the domain of validity of the one-loop result approaches the axis as r_3 increases.

We herewith rest our case.

8. Results and discussion

Having motivated our approach and justified our approximations in previous sections, we will now discuss our results. Most of them can be found in the figures of ref. [6], so instead of reproducing those figures, we tabulate the "raw" data i.e., the energies as functions of g, in tables 7 and 8.

Table 7 lists type IA and IB results, energy levels of the minimal hamiltonian diagonalised in a plane-wave or harmonic-oscillator basis. Recall from sect. 5 that the minimal hamiltonian incorporates a sixth order approximation for the one-loop potential along the vacuum valley, and only the lowest (fourth) order contribution

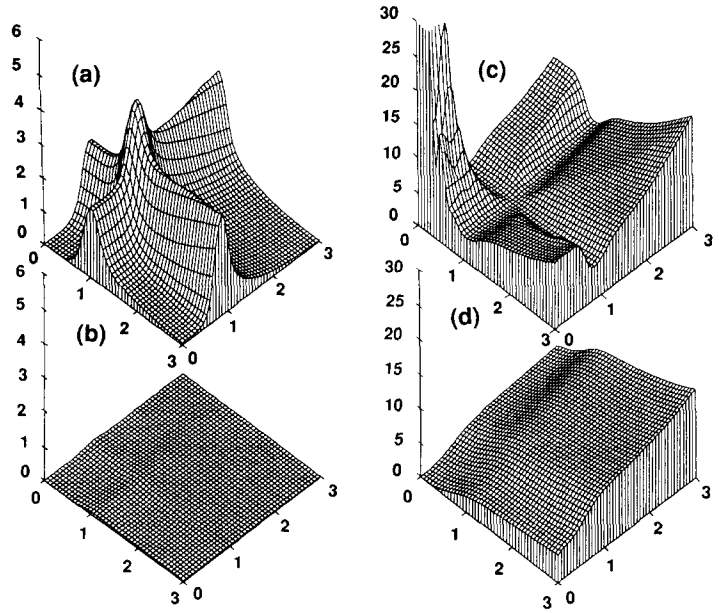

Fig. 10. Plots at $r_3 = 3$ as a function of r_1 and r_2 for (a) $(A_{k1}(C))^2$, (b) $(A^3_{k1}(C))^2$, (c) $L \cdot (V^{(2)}_{\rm tr}(C) - V^{(1)}_{\rm tr}(C))$ and (d) $L \cdot V^{(1)}_{\rm tr}(C)$.

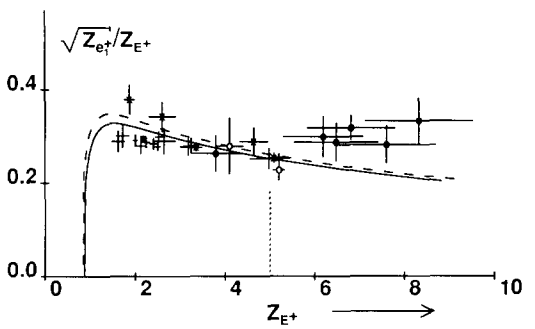

Fig. 11. The Monte Carlo data [20,27] compared with the Rayleigh-Ritz variational results for the energy of electric flux $\varepsilon_{E^+} = \Delta E/M(E^+)$, versus the distance $z_{E^+} = M(E^+) \cdot L$ (both in units of the glueball mass). Along the vertical axis we plot for easy comparison $\sqrt{\varepsilon_{E^+}/z_{E^+}} = \sqrt{z_{e_1^-}}/z_{E^+}$ which at *large* z_{E^+} can be identified with the square root of the string tension in units of the glueball mass. The crossed data points are from ref. [20], the open circles from ref. [27b] and the remaining data points are from ref. [27a] (see ref. [5] for details on the representation of the data from ref. [27]). The full line gives the Rayleigh-Ritz results for the minimal hamiltonian (type I(A&B)), the dashed line gives the Rayleigh-Ritz results for the full hamiltonian (type IIA) and the dotted line reminds us that we expect our approximations to break down beyond $z_{E^+} \sim 5$, presumably due to the onset of non-zero action tunneling.

TABLE 7
Type I(A&B) results for the energies (in units of $1/L$) of the lowest states in the listed O(3,Z) symmetry sectors, as well as for $(A_1^+)'$, the first excited state in the A_1^+ sector

g	A_1^+	$(A_1^+)'$	A_1^-	E^+	T_1^+	T_2^+	e_1^+	e_2^+	e_3^+
0.8	2.580(6)	3.540(450)	6.416(6)	3.458(165)		3.547(565)	2.586(15)	2.593(15)	2.596(1)
0.9	2.682(10)	3.651(550)	6.831(2)	3.558(142)		3.630(511)	2.698(10)	2.714(8)	2.729(1)
1.0	2.752(14)	3.763(650)	7.208(0)	3.656(72)	4.651(490)	3.661(472)	2.786(7)	2.821(4)	2.858(0)
1.1	2.792(13)	3.878(450)	7.544(0)	3.761(31)	4.915(142)	3.690(325)	2.853(5)	2.919(2)	2.990(0)
1.2	2.806(11)	3.999(350)	7.833(0)	3.873(18)	5.216(28)	3.719(151)	2.904(3)	3.010(1)	3.131(0)
1.3	2.800(6)	4.134(132)	8.070(1)	3.996(9)	5.550(16)	3.750(73)	2.942(2)	3.100(0)	3.287(0)
1.4	2.776(4)	4.285(83)	8.255(1)	3.783(6)	5.919(8)	3.783(22)	2.971(1)	3.192(0)	3.462(0)
1.5	2.739(2)	4.454(33)	8.390(1)	4.280(4)	6.323(6)	3.818(9)	2.996(1)	3.290(0)	3.660(0)
1.6	2.691(2)	4.641(12)	8.481(1)	4.444(3)	6.763(5)	3.857(7)	3.018(1)	3.399(0)	3.885(0)
1.8	2.565(1)	5.074(4)	8.552(2)	4.823(3)	7.754(4)	3.951(5)	3.068(1)	3.660(0)	4.424(0)
2.0	2.413(1)	5.590(2)	8.526(2)	5.277(2)	8.887(3)	4.073(4)	3.141(1)	3.999(0)	5.085(0)
2.2	2.251(1)	6.194(1)	8.481(2)	5.815(2)	10.157(3)	4.235(3)	3.256(1)	4.428(0)	5.864(0)
2.4	2.101(1)	6.884(1)	8.488(1)	6.442(1)	11.554(3)	4.446(3)	3.428(1)	4.949(0)	6.750(0)
2.6	1.981(1)	7.652(1)	8.594(1)	7.159(1)	13.071(4)	4.714(2)	3.663(1)	5.554(0)	7.728(0)
2.8	1.902(1)	8.486(1)		7.961(1)			3.961(1)		
3.0	1.870(1)	9.376(1)		8.837(1)			4.318(1)		
3.2	1.885(1)	10.314(1)		9.776(1)			4.725(1)		
3.4	1.942(1)	11.293(1)		10.767(1)			5.176(1)		

The lowerbound is obtained by subtracting the digits in parenthesis.

perpendicular to the vacuum valley. This is the simplest approximation one can expect to yield reasonably accurate values for the energies. Above $g = 1.2$ we used a basis of 500 plane waves (spherical Bessel functions), whereas below $g = 1.2$ we used up to 800 plane waves or harmonic oscillator wave functions to improve accuracy. Table 8 lists type IIA results, the full hamiltonian of sect. 3, diagonalised using plane waves. These tables also contain some new results, namely those for the T_1 representation, and for g values beyond 2.6 ($z_E > 5$).

We begin with a few words on the accuracy. For $(A_1^+)'$ (the first excited A_1^+ state), T_2^+, E^+ and T_1^+ we still have difficulty bringing the lower bound close to the upper bound, despite our use of the harmonic oscillator basis. Although there was substantial improvement at $g = 0.8$ and 0.9, it is likely that increasing $l_1 + l_2 + l_3$ beyond 20 will be much more helpful. Doing this is quite feasible, but it would be time consuming and is too academic to pursue. The reason is that in general the upper bound is much more accurate than the lower bound is willing to reveal. For example, at $g = 0.8$ the type IA result for T_2^+ is 3.611 (2572). The improvement lowers the upper bound by only 2%, but reduces the uncertainty by a factor 5. For the $(A_1^+)'$ at $g = 0.8$ we also find a 2% change, while for E^+ it is only 1%. However, for higher g the change is always less than 0.3%. Table 9 gives further evidence for an accuracy of better than 1% at low g values. There we list the energies

TABLE 8
Type IIA results, as in table 7

g	A_1^+	$(A_1^+)'$	A_1^-	E^+	T_1^+	T_2^+	e_1^+	e_2^+	e_3^+
0.8	2.558	3.486	6.389	3.419		3.502	2.569	2.572	2.575
0.9	2.646	3.576	6.790	3.489		3.557	2.664	2.681	2.698
1.0	2.698	3.665	7.147	3.564	4.546	3.559	2.735	2.774	2.814
1.1	2.713	3.752	7.456	3.644	4.784	3.558	2.781	2.852	2.931
1.2	2.699	3.843	7.710	3.727	5.054	3.554	2.805	2.921	3.054
1.3	2.659	3.944	7.902	3.817	5.355	3.547	2.812	2.985	3.190
1.4	2.598	4.057	8.032	3.915	5.686	3.539	2.808	3.047	3.343
1.5	2.518	4.184	8.102	4.024	6.048	3.529	2.794	3.112	3.517
1.6	2.423	4.325	8.116	4.145	6.444	3.518	2.774	3.185	3.717
1.8	2.187	4.654	8.000	4.426	7.336	3.497	2.727	3.367	4.199
2.0	1.904	5.055	7.750	4.770	8.359	3.486	2.690	3.620	4.800
2.2	1.591	5.533	7.462	5.187	9.506	3.498	2.684	3.958	5.516
2.4	1.276	6.091	7.222	5.688	10.771	3.547	2.728	4.384	6.335
2.6	0.982	6.719	7.087	6.274	12.215	3.643	2.831	4.891	7.243
2.8	0.725	7.405		6.939			2.994		
3.0	0.511	8.140		8.469			3.211		
3.2	0.341	8.914		9.308			3.475		
3.4	0.209	9.722		10.181			3.777		

These include all corrections discussed in the text.

TABLE 9
Type I(A&B) results for the first excited A_1^+ and the lowest T_2^+ state with 0 and 3 units of electric flux, compared with the perturbative prediction E_P [3]

	$(A_1^+)'$				T_2^+			
g	$E(0,0,0)$	$E(1,1,1)$	$\bar{E}$	E_P	$E(0,0,0)$	$E(1,1,1)$	$\bar{E}$	E_P
0.5	3.105(420)	3.109(173)	3.107	3.103				
0.55	3.213(410)	3.244(128)	3.228	3.230				
0.6	3.297(374)	3.376(110)	3.336	3.342				
0.65	3.365(342)	3.510(101)	3.437	3.441				
0.7	3.427(352)	3.649(91)	3.538	3.527	3.431(532)	3.487(153)	3.459	3.458
0.8	3.540(450)	3.949(61)	3.744	3.662	3.547(565)	3.712(140)	3.629	3.603
0.9	3.651(550)	4.289(31)	3.970	3.752	3.630(571)	3.944(26)	3.787	3.761
1.0	3.764(650)	4.674(12)	4.219	3.809	3.661(472)	4.199(5)	3.930	3.819
1.2	3.999(350)	5.588(1)	4.794	3.780	3.719(325)	4.799(0)	4.259	3.904

The quantity $\bar{E}$ is the average $\frac{1}{2}(E(0,0,0) + E(1,1,1))$, and we expect $E_P - \bar{E} = O((E(1,1,1) - E(0,0,0))^2)$. All energies are in units of $1/L$.

for $(A_1^+)'_{e=0}$, $(A_1^+)'_{e=(1,1,1)}$, $(T_2^+)_{e=0}$, $(T_2^+)_{e=(1,1,1)}$, the average of these two energies for each representation, and the perturbative prediction of Lüscher and Münster [3]. As explained in sect. 6, the average should equal the perturbative result, up to corrections vanishing rapidly once tunneling effects are small. The agreement is extremely good. Table 9 also shows that for $(A_1^+)'$ (and E^+) tunneling sets in around $g = 0.5$, but somewhat later for T_2^+.

We now come to the new results for the T_1^+ representation. This is an important state because it confronts one with an issue, which is as follows. In a situation where the cubic group can be enlarged to the full rotation group, the irreducible representations we have been discussing combine into angular momentum multiplets, a fact used extensively in the Monte Carlo analysis [21]. In particular, in a large volume one expects restoration of rotational invariance, both on the lattice and in our continuum calculation on a torus. One therefore conjectures that the energy gap between each representation $R \neq A_1^+$ and the A_1^+ groundstate (which is the true vacuum) gives the mass of the lowest angular momentum state containing R (and $(A_1^+)'$ supposedly gives the 0^+ mass). Thus, in refs. [20] and [21], spin 2 is associated with the E and T_2 representations, spin 1 with the T_1, and spin 3 with the A_2 representation. On these grounds, it is tempting to conjecture that our T_1^+ state will correspond in larger volumes to a spin 1 state, especially since they are both triplets.

The above claim apparently contradicts a statement by Lüscher and Münster [3] that the $J = 1$ states cannot be studied within the context of the zero-momentum effective hamiltonian. The resolution of this contradiction shows one must at least be careful about simplisticly deducing infinite volume results from our intermediate volume energies. Lüscher and Münster observe that the lowest order effective hamiltonian, valid at small g, possesses full rotational symmetry, and give an argument that in general prohibits any odd spin multiplets from forming as $g \to 0$. However, this symmetry is in a sense accidental, and there is no reason why the energy levels should combine into multiplets in the same way at $g \to 0$ as in the infinite volume limit.

The question thus arises, to what spin multiplet the T_1^+ (and A_2^+) belong as $g \to 0$. This can be answered as follows. The lowest order effective hamiltonian is what we have called the truncated ("type III") hamiltonian, and one can scale out g, where upon taking $g \to 0$ is equivalent to moving the boundary condition to infinity. Thus we have a problem of type IIIC, in the language of sect. 5. One can find the eigenstates, and settle the low g spin assignments by identifying degeneracies between different representations of the cubic group. In table 10 we collect the results. The conclusion is that T_1^+ and A_2^+ belong to $J = 4$ and $J = 6$ respectively.

As mentioned above, there is no reason to expect these spin assignments to hold for a large volume, and the reason we wish to be cautious about identifying our results at $z_{E^+} \sim 5$ with certain spin states is that the volumes we probe are still too small to restore rotational invariance. This is clear from the fact that the E^+ and T_2^+ groundstates differ substantially in energy. However, the level rearrangements

TABLE 10
Low g spin assignments. $\epsilon_1 = L \cdot E/g^{2/3}$, computed using type IIIC at $g = 1$

J	ϵ_1	R
$0+$	4.1167(0)	A_1^+
2^+	6.0145(47)	E^+, T_2^+
0^+	6.3863(0)	A_1^+
4^+	7.7355(103)	A_1^+, E^+, T_1^+, T_2^+
2^+	7.822(10)	E^+, T_2^+
0^+	7.974(0)	A_1^+
0^-	8.7867(0)	A_1^-
0^+	9.25...	A_1^+
6^+	9.3273(241)	A_1^+, A_2^+, E^+, T_1^+, $2 \times T_2^+$
2^-	11.331(0)	E^-, T_2^-
0^-	12.055(2)	A_1^-
4^-	13.721(27)	A_1^-, E^-, T_1^-, T_2^-
6^-	15.988(39)	A_1^-, A_2^-, E^-, T_1^-, $2 \times T_2^-$

We list only the eight lowest even parity states and five lowest odd parity states.

are somewhat restricted because we do not expect crossing of levels *within* a representation of the cubic group, since O(3, Z) is a good symmetry at all values of the coupling. This indeed makes it very tempting to identify $(A_1^+)'$ with $J^P = 0^+$, T_1^+ with $J^P = 1^+$, E^+ and T_2^+ with $J^P = 2^+$, A_2^+ with $J^P = 3^+$ and A_1^- with $J^P = 0^-$. It supports the conjecture made in ref. [20] that the 2^+ glueball mass is lower than the 0^+ mass, which is allowed by rigorous mass inequalities [22]. But again we emphasize that we do not yet know how, for example, the E^+ and T_2^+ will merge into a 2^+ multiplet at large volumes. The natural choice for the 2^+ mass as a "weighted" average of the E^+ and T_2^+ mass might require "negative weights."

We now move on to a discussion of mass ratios, expressed as functions of z, the renormalization-group-independent parametrisation of the box size. As was stressed in ref. [6], we consider these results to be particularly reliable. For a given representation R, one can define

$$z_R = L \cdot M_R = L \cdot \left(E_R - E_{A_1^+} \right). \tag{8.1}$$

We chose $z_{A_1^+} = L \cdot (E_{(A_1^+)'} - E_{A_1^+})$ as our parameter in refs. [5,17], and z_{E^+} in ref. [6]. This allowed easy comparison with the Monte Carlo results of ref. [20]. The mass ratios can be expressed as z_{R_1}/z_{R_2}, and we will always relate masses to z_{E^-}. In ref. [6] we found $z_{A_1^+}/z_{E^+} \sim 1.1$ and $z_{T_2^+}/z_{E^+} \sim 0.50$, both almost constant over the range $z_{E^+} = 2$–5. A similar constant behaviour occurs for T_1^+: $z_{T_1^+}/z_{E^+} \simeq 2.1$, easily deduced from tables 7 and 8. Again [6], the higher order corrections included in table 8 lead to less than a 1% change in $z_{T_1^+}/z_{E^+}$. For A_1^- we observed a strong volume dependence, with $z_{A_1^-}/z_{E^+}$ dropping from ~ 5 at $z_{E^+} \sim 1$ to ~ 1 at $z_{E^+} \sim 5$.

We have drawn the line on producing detailed results at A_2 (for which $z_{A_2^+}/z_{E^+} \sim 3.6$) and at $z_{E^+} = 5$. The former needs no justification, but the latter choice is of crucial importance. Thus tables 7 and 8 contain some results beyond this point. Let us first remind the reader of the physical reasons we have to expect our approximations to break down at $z_{E^+} \simeq z_{A_1^+} \simeq 5$. It is the distance where the energy for the Nambu-Goto string becomes imaginary, and it is the distance scale set by the deconfining temperature T_c [7, 16, 23, 24, 25]. A more technical reason is that there is still one feature we have not incorporated in the effective hamiltonian, which is the presence of non-zero-action instantons, i.e., the θ-dependence of the energies [26]. In analogy to the present case of zero-action instantons, where the energy of electric flux is the most suitable quantity for detecting the onset of tunneling, the topological susceptibility χ_t is the most suitable quantity for detecting the onset of non-zero-action tunneling. Although the energy levels will depend smoothly on g as this tunneling sets in, just as in the present case, their values will deviate substantially from the values obtained when neglecting these tunneling contributions. Thus the true energies will begin to deviate from the energies we calculate here, just like our energies began to deviate from the perturbative formulae of Lüscher and Münster. Indeed, if we consider the results in tables 7 and 8 beyond $z_{E^+} = 5$, we do find a deviation from the Monte Carlo results. To illustrate this we reproduce in fig. 11 the fig. 2 of ref. [5] (which was based on the data of ref. [27]). We augment the figure with Monte Carlo data from ref. [20] and our results from tables 7 (full line) and 8 (dashed line). (We have assumed, as was done in ref. [28], that the masses listed in ref. [27a] are for the $E(2^+)$ and not the $A_1(0^+)$ state. This will be true if the $E(2^+)$ is far enough below the $A_1(0^+)$ so that there was only one intermediate state in the correlation measured in ref. [27a].)

In ref. [24] one of us mused on the usefulness of studying volume dependence of χ_t, conjecturing that χ_t drops to zero when approaching $z \simeq 5$ from above. Actually, those investigations had already been done, in the guise of a study of temperature dependence [29, 30]. The results are however conflicting. Without passing judgement on calculations as complex as these, we consider the results of ref. [29], which do show strong suppression of χ_t in the deconfined phase, to be more appealing, because they are based directly on instanton dynamics. Direct analogues of instantons occur in lattice gauge theory as (approximate) saddle points in the action, and there is no need to take a continuum limit to use the concept.

All of these arguments strengthen our belief that $z_{E^+} = 5$ is where all the action is. What the dynamics is, we can now only guess. One guess would be the formation (driven by non-zero-action instanton effects) of domains with a size corresponding to $z \sim 5$. An electric flux string might then comprise "beads" of domains with $\boldsymbol{e} \neq \boldsymbol{0}$ (a picture surprisingly similar to the proposal in [31]). After all, the energy of electric flux per unit length we have calculated is remarkably close to the string tension. Rotational invariance could be restored as in the Copenhagen vacuum [32] or the Ising model. Such domains would be magnetically neutral. An updated

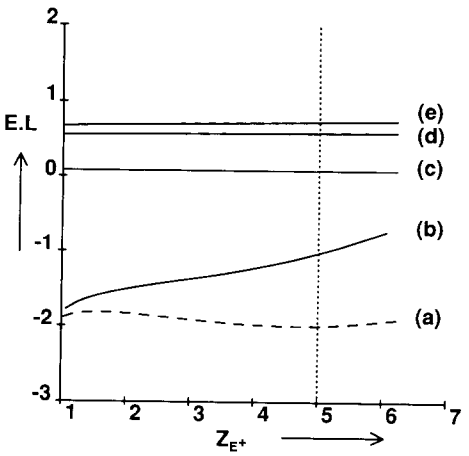

Fig. 12. The chromomagnetic energies to two loops [9] compared with the magnetically neutral vacuum energies on a torus. The dashed line (a) is the vacuum energy $E(A_1^+)$ obtained from table 8, which includes the higher order corrections to the effective hamiltonian, whereas the full line (b) gives $E(A_1^+)$ from table 7, where higher order corrections were ignored. The vacuum energies for non-zero magnetic flux $\boldsymbol{m} \in Z_2^3$ are labelled (c) for $\boldsymbol{m} = (1,0,0)$, (d) for $\boldsymbol{m} = (1,1,0)$ and (e) for $\boldsymbol{m} = (1,1,1)$.

version of fig. 3 in ref. [9], which is presented in fig. 12, seems to indicate this. In this figure, the chromomagnetic energies on a torus are compared with the magnetically neutral vacuum energy. The latter was obtained from table 7 (full line) and table 8 (dashed line) by adding the "zero field" contribution (see sect. 3 and ref. [9]):

$$\left(-2a(4)/\pi^2 + \tfrac{3}{8}\left(a(2)g/\pi^2\right)^2\right)L^{-1} = \left(-5.025221 + 27\kappa_1^2 g^2/8\right)L^{-1}. \quad (8.2)$$

Since the energy of the magnetically neutral state is always lower than the chromomagnetic energies, magnetically neutral domains in the scenario of ref. [9] seem to be preferred. Of course, this argument could be affected by higher order corrections and the effects of non-zero-action instantons.

Things are however not as simple as they seem. The duality relations of 't Hooft [1] put important constraints on the behaviour of chromomagnetic energies in large volumes, and 't Hooft's algebra for the A and B operators [33] rules out a vacuum of *uncorrelated* domains. These fundamental constraints are of a kinematic nature, and deserve more attention in building a model (or even a picture) for the Yang-Mills vacuum. They will be indispensable for understanding what confinement is about, and cannot be ignored.

Another important issue will be the connection with Lüscher's large volume expansion for the glueball mass [34]. The expected [3, 35] plateau for the glueball mass M as a function of z found in ref. [6] cannot, however, be interpreted as the

infinite volume glueball mass for three reasons. First, as we mentioned before, there is no restoration of rotational symmetry below $z_E \sim 5$. Second, we used the two-loop beta function to convert z to a physical mass, which for $g \sim 2.6$ is certainly questionable (higher loop calculations for both the beta function [36] and our effective hamiltonian are required to establish the accuracy). Third, and physically more important, Lüscher's result predicts the asymptotic value will be reached from below. We therefore expect a dip to occur in $M(z)$ around $z \sim 5$. Interestingly, this has been observed [37] for the available SU(3) Monte Carlo data.

In conclusion, we believe we now understand the dynamics of non-abelian gauge theories in intermediate volumes, and that our present calculations have brought us to the point where confinement and restoration of rotational symmetry sets in. Only now can we meaningfully start to ask what the dynamical contribution of non-zero-action instantons will be. Necessarily this question needs to be addressed outside the sector of zero momentum configurations. But the latter might still play an important role if indeed domain formation occurs as we speculated above. We hope that the methods we have developed to include pinchons (the zero-action instantons) can be adapted to include the non-trivial topology classified by the Pontryagin number (eq. (1.7)).

We are grateful to Werner Nahm for a discussion on Gribov ambiguities and for his encouragement. We thank Jos Vermaseren for the check on part of our algebraic manipulations. This work was supported in part by NSF grant numbers DMS-84-05661 and PHY-85-07627 and by DOE grant number DE-FG03-85ER25009.

Appendix A

We give here a number of useful SU(2) and lattice sum identities, used in the background field calculation. We use the following notation: If A is an SU(2) Lie algebra element,

$$A \equiv A^a \frac{\sigma^a}{2}, \tag{A.1}$$

then in the adjoint representation its matrix is $\mathbf{A} \equiv \mathrm{ad}\, A$ where

$$\mathbf{A}^{ab} = -i\varepsilon_{abc} A^c. \tag{A.2}$$

Thus the adjoint matrices act on the Lie algebra vectors as

$$\mathbf{B}A \equiv [B, A]. \tag{A.3}$$

The following identities reduce the traces of products of adjoint matrices in eq.

(2.14) to inner products of Lie algebra vectors. The fundamental results are

$$\mathbf{AB} = A \cdot B\mathbf{1} - BA^{\mathrm{T}},$$

i.e.,

$$(\mathbf{AB})^{ab} = (A^c B^c)\delta^{ab} - B^a A^b,$$

$$\mathbf{F}_{ij} = i\left(c_i c_j^{\mathrm{T}} - c_j c_i^{\mathrm{T}}\right),$$

$$F_{ij} \cdot c_k = -\varepsilon_{ijk}(\det c). \tag{A.4}$$

For the product of four adjoint matrices, Lüscher [3] has already given useful identities, so we will only discuss products of six adjoint matrices.

$$\begin{aligned}\mathrm{Tr}\left[(\boldsymbol{c}_i)^2(\boldsymbol{c}_j)^2(\boldsymbol{c}_k)^2\right] &= 3(c_i \cdot c_j)^2(c_l \cdot c_l) - (c_i \cdot c_j)(c_j \cdot c_k)(c_i \cdot c_k) \\ &= 2(c^2)^3 - \tfrac{3}{2}F^2c^2 - 3(\det c)^2, \end{aligned} \tag{A.5}$$

$$\begin{aligned}\mathrm{Tr}\left[(\boldsymbol{c}_i)^2\boldsymbol{c}_j(\boldsymbol{c}_k)^2\boldsymbol{c}_j\right] &= (c_i \cdot c_i)^3 + 2(c_i \cdot c_j)(c_j \cdot c_k)(c_i \cdot c_k) - (c_i \cdot c_j)^2(c_k \cdot c_k) \\ &= 2(c^2)^3 - 2F^2c^2 + 6(\det c)^2, \end{aligned} \tag{A.6}$$

$$\begin{aligned}\mathrm{Tr}[\boldsymbol{c}_i\boldsymbol{c}_j\boldsymbol{c}_k\boldsymbol{c}_j\boldsymbol{c}_i\boldsymbol{c}_k] &= 2(c_i \cdot c_j)(c_j \cdot c_k)(c_i \cdot c_k) \\ &= 2(c^2)^3 - 3F^2c^2 + 6(\det c)^2. \end{aligned} \tag{A.7}$$

Here we sum over indices occurring more than once, unless an explicit summation symbol shows otherwise. Note that rotationally invariant expressions such as those above can be written in terms of the three independent rotationally and gauge invariant objects

$$c^2 = \left(c_i^a\right)^2 = x_i^2,$$

$$F^2 = \left(F_{ij}^a\right)^2 = \sum_{i \neq j} x_i^2 x_j^2,$$

$$\det c = x_1 x_2 x_3. \tag{A.8}$$

Here x_i are the polar coordinates [4] of the matrix c_i^a, i.e., with a suitable rotation and gauge transformation c_i^a can be made diagonal with x_i on the diagonal. Other

rotational invariants are:

$$\mathrm{Tr}\left[(\mathbf{F}_{ij})^2(\boldsymbol{c}_k)^2\right] = (F_{ij}\cdot F_{ij})(c_k\cdot c_k) + (F_{ij}\cdot c_i)^2$$

$$= F^2c^2 + 6(\det c)^2, \tag{A.9}$$

$$\mathrm{Tr}\left[(\mathbf{F}_{ij}\boldsymbol{c}_k)^2\right] = 2(F_{ij}\cdot c_k)^2 = 12(\det c)^2, \tag{A.10}$$

$$\mathrm{Tr}\left[\mathbf{F}_{ij}\mathbf{F}_{jk}\mathbf{F}_{ki}\right] = -6i(\det c)^2. \tag{A.11}$$

Thus we are left with the last two terms in eq. (2.13), which break the rotational invariance. The following momentum sums occur:

$$p = \sum_{\boldsymbol{k}} \frac{1}{|\boldsymbol{k}|^5}, \qquad q = \sum_{\boldsymbol{k}} \frac{k_i^4}{|\boldsymbol{k}|^9},$$

$$r = \sum_{\boldsymbol{k}} \frac{k_i^6}{|\boldsymbol{k}|^{11}}, \qquad s = \sum_{\boldsymbol{k}} \frac{k_i^2k_j^2}{|\boldsymbol{k}|^9},$$

$$t = \sum_{\boldsymbol{k}} \frac{k_1^2k_2^2k_3^2}{|\boldsymbol{k}|^{11}}, \qquad u = \sum_{\boldsymbol{k}} \frac{k_i^2k_j^4}{|\boldsymbol{k}|^{11}}. \tag{A.12}$$

In these expressions i and j are fixed and unequal but q, r, s and u do not depend on their value. They are related as follows:

$$s = \tfrac{1}{6}p - \tfrac{1}{2}q,$$

$$t = \tfrac{1}{6}p + r - \tfrac{3}{2}q,$$

$$u = \tfrac{1}{2}q - \tfrac{1}{2}r. \tag{A.13}$$

We find:

$$\sum_{\boldsymbol{k}} \frac{k_ik_jk_kk_l}{|\boldsymbol{k}|^9}\mathrm{Tr}\left[(\boldsymbol{c}_n)^2\boldsymbol{c}_i\boldsymbol{c}_j\boldsymbol{c}_k\boldsymbol{c}_l\right]$$

$$= (q-3s)\sum_i \mathrm{Tr}\left[(\boldsymbol{c}_j)^2(\boldsymbol{c}_i)^4\right]$$

$$+ s\left(\mathrm{Tr}\left[\left((\boldsymbol{c}_i)^2\right)^3\right] + 2\,\mathrm{Tr}\left[(\boldsymbol{c}_i)^2\boldsymbol{c}_j(\boldsymbol{c}_k)^2\boldsymbol{c}_j\right] - \tfrac{1}{2}\,\mathrm{Tr}\left[(\boldsymbol{c}_i)^2(\mathbf{F}_{jk})^2\right]\right) \tag{A.14}$$

and

$$\sum_{k} \frac{k_i k_j k_k k_l k_m k_n}{|k|^{11}} \mathrm{Tr}[c_i c_j c_k c_l c_m c_n]$$

$$= (r - 15u + 30t) \sum_i \mathrm{Tr}\left[(c_i)^6\right]$$

$$+ 3(u - 3t) \sum_j \left(2\,\mathrm{Tr}\left[(c_i)^2 (c_j)^4\right] + 2\,\mathrm{Tr}\left[c_i (c_j)^3 c_i c_j\right] + \mathrm{Tr}\left[c_i (c_j)^2 c_i (c_j)^2\right]\right)$$

$$+ t\left(2\,\mathrm{Tr}\left[(c_i)^2 (c_j)^2 (c_k)^2\right] + 6\,\mathrm{Tr}\left[(c_i c_j)^2 (c_k)^2\right] + 3\,\mathrm{Tr}\left[c_i (c_j)^2 c_i (c_k)^2\right]\right.$$

$$\left. + \mathrm{Tr}\left[(c_i c_j c_k)^2\right] + 3\,\mathrm{Tr}[c_i c_j c_k c_j c_i c_k]\right). \quad \text{(A.15)}$$

The rotationally invariant terms have been listed already, except for one, which is readily reduced to known ones:

$$\mathrm{Tr}\left((c_i c_j c_k)^2\right) = \mathrm{Tr}(c_i c_j c_k c_j c_i c_k) - \tfrac{1}{2}\,\mathrm{Tr}\left((F_{ij} c_k)^2\right). \quad \text{(A.16)}$$

Similar manipulations yield:

$$2 \sum_j \mathrm{Tr}\left[c_i (c_j)^3 c_i c_j\right] = \sum_j \left(\mathrm{Tr}\left[(c_i)^2 (c_j)^4\right] - \mathrm{Tr}\left[(c_j)^2 (F_{ij})^2\right] + \mathrm{Tr}\left[c_i (c_j)^2 c_i (c_j)^2\right]\right). \quad \text{(A.17)}$$

The following four identities complete the conversion to the invariants of eq. (2.15).

$$\sum_i \mathrm{Tr}\left[(c_i)^6\right] = 2 \sum_i (c_i \cdot c_i)^6, \quad \text{(A.18)}$$

$$\sum_j \mathrm{Tr}\left[(c_i)^2 (c_j)^4\right] = \sum_j \left(2(c_j \cdot c_j)^2 (c_i \cdot c_i) - (F_{ij} \cdot F_{ij})(c_j \cdot c_j)\right), \quad \text{(A.19)}$$

$$\sum_j \mathrm{Tr}\left[(c_j)^2 (F_{ij})^2\right] = \sum_j (F_{ij} \cdot F_{ij})(c_j \cdot c_j), \quad \text{(A.20)}$$

$$\sum_j \mathrm{Tr}\left[c_i (c_j)^2 c_i (c_j)^2\right] = 2 \sum_j \left((c_i \cdot c_i)(c_j \cdot c_j) - (F_{ij} \cdot F_{ij})\right)(c_j \cdot c_j). \quad \text{(A.21)}$$

As mentioned in sect. 2, one can also write the one-loop effective potential in terms of the invariants $M_{ij} = c_i \cdot c_j$, which is the form in which we obtained the sixth

order term using a symbolic manipulation programme:

$$V_1^{(6)} = \left(\tfrac{17}{48}p - \tfrac{35}{16}s + \tfrac{21}{8}t\right)(\mathrm{Tr}[M])^3 + \left(\tfrac{36}{4}t - \tfrac{1}{3}p - \tfrac{105}{16}s\right)\mathrm{Tr}[M]\mathrm{Tr}[M^2]$$
$$+\left(\tfrac{119}{8}s - \tfrac{35}{48}p - \tfrac{441}{16}t\right)\mathrm{Tr}[M]\sum_i M_{ii}^2 + \left(\tfrac{23}{48}p - \tfrac{35}{8}s + 21t\right)\mathrm{Tr}[M^3]$$
$$+\left(\tfrac{427}{16}s - \tfrac{35}{48}p - \tfrac{441}{4}t\right)\sum_i M_{ii}(M^2)_{ii} + \left(\tfrac{7}{8}p - \tfrac{441}{16}s + \tfrac{1617}{16}t\right)\sum_i (M_{ii})^3. \quad \text{(A.22)}$$

Appendix B

In this appendix we discuss the perturbative, semiclassical, variational and Monte Carlo analyses performed as a feasibility and warm-up study for SU(2). The model is the 2-dimensional vacuum valley of ref. [7]:

$$H = -\frac{g^2}{2}\left(\frac{\partial^2}{\partial X^2} + \frac{\partial^2}{\partial Y^2}\right) + \frac{1}{2g^2}(X^2-1)^2Y^2. \quad \text{(B.1)}$$

The perturbative expansion for the well at $X = 1$ is obtained by substituting

$$X = g^{2/3}x + 1,$$
$$Y = g^{2/3}y, \quad \text{(B.2)}$$

giving:

$$g^{-2/3}H = -\frac{1}{2}\left(\frac{\partial^2}{\partial x^2} + \frac{\partial^2}{\partial y^2}\right) + 2x^2y^2 + 2g^{2/3}x^3y^2 + \tfrac{1}{2}g^{4/3}x^4y^2. \quad \text{(B.3)}$$

The energy eigenvalues are classified by the parity in y, and were calculated using a Rayleigh-Ritz algorithm. Our basis was $\Psi(x, y) = \langle x|n; w_x\rangle\langle y|m; w_y\rangle = \langle x, y|n, m\rangle$, where $\langle x|n; w\rangle$ are 1-dimensional harmonic oscillator eigenfunctions, and the frequencies w_x and w_y were used as variational parameters. The resulting perturbative expansions for the ground-state energy in the even(+) and odd(−) y-parity sectors are:

$$E^+(g) = 0.87959730g^{2/3} - 0.21065396g^2 + \mathrm{O}(g^{8/3}),$$
$$E^-(g) = 1.8879261g^{2/3} - 0.23230415g^2 + \mathrm{O}(g^{8/3}). \quad \text{(B.4)}$$

The lowest order result is obtained by diagonalising the matrix of H_0 in the appropriate sector, where H_0 is the single-well hamiltonian [7]:

$$H_0 = -\frac{1}{2}\left(\frac{\partial^2}{\partial x^2} + \frac{\partial^2}{\partial y^2}\right) + 2x^2y^2. \quad \text{(B.5)}$$

For these ground states, which are even in x, the first order correction vanishes because the first order term in H is odd in x. Thus we can write

$$\Psi^{\pm} = \Psi_0^{\pm} + g^{2/3}\Psi_1^{\pm} + \cdots ,$$

$$E^{\pm} = g^{2/3}E_0^{\pm} + g^2 E_2^{\pm} + \cdots ,$$

$$H = g^{2/3}H_0 + g^{4/3}H_1 + g^2 H_2 ,$$

$$H_1 = 2x^3 y^3 ,$$

$$H_2 = \tfrac{1}{2}x^4 y^2 . \tag{B.6}$$

We briefly discuss our approach to computing E_2, since a similar method is used in sect. 7. In general

$$E_2^{\pm} = \langle \Psi_0^{\pm} | H_1 | \Psi_1^{\pm} \rangle + \langle \Psi_0^{\pm} | H_2 | \Psi_0^{\pm} \rangle , \tag{B.7}$$

and a useful observation is that we can obtain $\Psi_1^{\pm}$ by using a routine from the IMSL library to solve the linear equation

$$\left(H_0 - E_0^{\pm}\right)\Psi_1^{\pm} = -H_1\Psi_0^{\pm} . \tag{B.8}$$

This avoids having to find all eigenvalues and eigenvectors of H_0. The point is simply that $\Psi_1^{\pm}$ and $H_1\Psi_0^{\pm}$ are odd in x, so we can restrict eq. (B.8) to the odd x-parity sector where it is non-singular. It is then easily written as a matrix equation in our Rayleigh-Ritz basis, and solved. Eq. (B.4) was calculated using up to 351 basis vectors and $w_x = w_y \sim 2.0$.

Next we discuss the semiclassical analysis. The perturbative ground state wave function in the well at $X = +1$ must be combined with one at $X = -1$, and an energy split appears between the even and odd x-parity combinations. Energies will thus be classified by the x-parity and y-parity, with the notation $E^{(x\text{-parity})(y\text{-parity})}$. Perturbatively one has $E^{+\pm} = E^{-\pm} = E^{\pm}$. The result for the ground-state energy split obtained in ref. [7] was

$$\begin{aligned} \Delta E &= \left(E^{++} - E^{-+}\right) \\ &= 2g^{2/3}|C(g)|^2 \exp\left(-\tfrac{1}{2}\pi g^{-1} + \varepsilon_0 g^{-1/3}\pi\right), \end{aligned} \tag{B.9}$$

(note the typing error in eq. (5.45) of ref. [7]). Here all corrections are absorbed into the definition of $C(g)$, and ε_0 is the lowest order perturbative energy, calculated from (B.4) to be $\varepsilon_0 = \lim_{g\to 0} g^{-2/3}E^{+} = 0.87959730\ldots$. As in sect. 6 we rewrite this

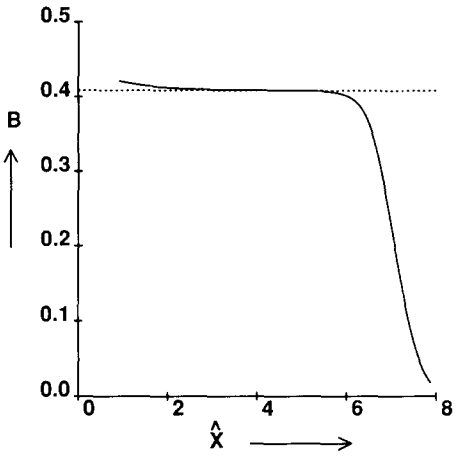

Fig. 13. The Rayleigh-Ritz results for the asymptotics of the single-well wave function as defined in eq. (B.12).

equation as

$$\Delta E = (1+f''(g))^{-1} 2g^{2/3}|C|^2 \exp\left(\frac{\pi}{2g}(E^{++}+E^{-+}-1)\right), \tag{B.10}$$

where $f''(g) \to 0$ as $g \to 0$, and C is the coefficient of the asymptotic form of the perturbative wave function along the vacuum valley $y = 0$ (eq. (5.46), ref. [7]):

$$C = \lim_{x\to\infty} C(x),$$

$$C(x) \equiv \frac{(2x)^{1/2}}{\pi^{1/4}} \exp\left(\tfrac{1}{3}(2x-2\varepsilon_0)^{3/2}\right) \int \mathrm{d}y\, \Psi_0^+(x,y) \mathrm{e}^{-xy^2}. \tag{B.11}$$

We must thus evaluate $\Psi_0(x, y)$ to high accuracy and apply the above projection. As in the SU(2) case of ref. [4], we cannot explicitly take the $x \to \infty$ limit because the tail of the wave function is inaccurate. However, for large enough x we expect $C(x)$ to be almost constant, and the point where this occurs can be shifted to smaller x by including analytic corrections to the asymptotic form divided out in (B.11). Thus in fig. 13 we plot

$$B(x) = C(x)/h(x), \tag{B.12}$$

where $h(x)$ is asymptotically 1 and satisfies

$$\left(-\frac{1}{2}\frac{\mathrm{d}^2}{\mathrm{d}x^2} + x + \frac{1}{16x^2}\right) h(x) = \varepsilon_0 h(x). \tag{B.13}$$

We see $B(x)$ indeed stabilises rapidly to a constant value, until numerical inaccu-

TABLE 11
The Rayleigh-Ritz results for the toy model. $f''(g)$ is defined in eq. (B.13) and $E^{\pm}$ are given in eq. (B.4)

g	E^{++}	E^{-+}	$E^{-+}-E^{++}$	$f''(g)$	$\frac{1}{2}(E^{++}+E^{-+})$	$E^{+}(g)$	E^{+-}	$E^{-}(g)$
0.09	0.17487575	0.17487654	0.00000079	−0.0014	0.17487615	0.17494313	0.37724	0.3772703
0.1	0.18729819	0.18730214	0.00000395	−0.0158	0.18730016	0.18739695	0.40437	0.4044183
0.2	0.2890532	0.2933515	0.0043107	−0.0016	0.29120238	0.29239189	0.635790	0.6363695
0.25	0.3256065	0.3414209	0.0158144	0.0327	0.33351369	0.33590255	0.733062	0.7347050
0.3	0.3540396	0.3901446	0.0361050	0.0842	0.3720921	0.37522430	0.820595	0.8251487
0.35	0.3770573	0.4407058	0.0636485	0.1483	0.4088816	0.41104178	0.898229	0.9091703
0.4	0.3969677	0.4935331	0.0965654	0.2193	0.4452504	0.44381425	0.965727	0.9877553
0.45	0.4152398	0.5487022	0.1334624	0.2935	0.4819710	0.47386862	1.023656	1.0616055
0.5	0.4327243	0.6061322	0.1734079	0.3685	0.5194283	0.50144809	1.073428	1.1312429

racy causes it to drop to zero. We thus obtain

$$C = 0.4083 \pm 0.0002 \tag{B.14}$$

from the plateau in fig. 13, which is data from the perturbative variational calculation with 351 basis vectors and $w_x = w_y = 2$.

We wish now to compare these predictions with a Rayleigh-Ritz analysis of the full hamiltonian, eq. (B.1). Note how this differs from the perturbative calculation, where we applied the Rayleigh-Ritz method to only the single well hamiltonian H_0 in eq. (B.3). As a basis we again took products of harmonic oscillator eigenfunctions in the x and y directions.

Despite the fact that our x-oscillators are centered at $X = 0$ (whereas at small g values the wave functions are localised around $X = \pm 1$) we could obtain accurate results even at low values of g. This was achieved by tuning w_x and w_y separately, and we never required more than 231 basis vectors. Table 11 lists the results, showing the number of digits we believe to be significant, although no rigorous bounds were calculated for this toy model. We find very good agreement with the perturbative and semiclassical predictions, and observe that $f''(g) = \mathrm{O}(\Delta E(g))$, just as anticipated in sect. 6. Actually, $f''(g)$ is remarkably well fitted by $f''(g) \simeq 2.3\Delta E(g)$, given that uncertainty in C leads to an error of ± 0.001 in $f''(g)$. This therefore substantiates our claim in sect. 6 that the perturbative factor $f(g)$ in the semiclassical formula has no $\mathrm{O}(g^{2/3})$ term and is determined by the transverse fluctuation along the pinchon, leading to $\mathrm{O}(g)$ corrections for SU(2) and $\mathrm{O}(\Delta E(g))$ corrections for the toy model. Table 11 also shows that $\frac{1}{2}(E^{++}+E^{-+})$ and E^{+-} agree with the perturbative predictions $E^{\pm}(g)$ of eq. (B.4) to high precision.

We end this appendix with a short discussion of the Monte Carlo analysis we carried out for the toy model. We follow in detail the approach described in refs. [38, 39]. The time step size (a) varied from 0.2 to 0.5, and the number of sites (N) in the time direction was usually 10 000. For some runs we took $N = 1000$ to

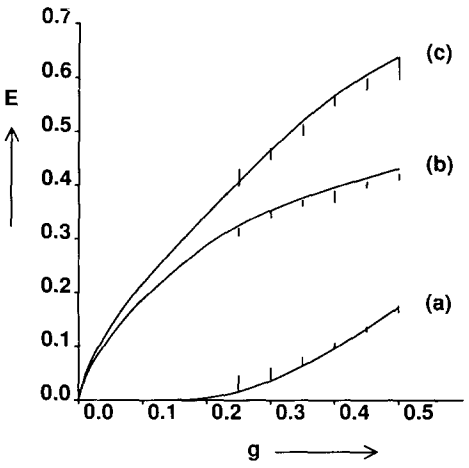

Fig. 14. Rayleigh-Ritz and Monte Carlo results for the toy-model energies: (a) $\Delta E = E^{-+} - E^{++}$, (b) E^{++} and (c) E^{+-}.

investigate temperature dependence. We averaged over $N_E = 100$ ensembles, sampling occurring every 5th sweep through the time lattice. We used $\bar{n} = 5$ Metropolis hits per site, and intervals $|x - x'| \leqslant \Delta_x$ and $|y - y'| \leqslant \Delta_y$ were chosen for updating, with $\Delta_x = \Delta_y = 2g\sqrt{a}$. Finally, $N_T = 500$ sweeps were performed before starting to sample, to ensure thermalisation. To check on thermalisation, we calculated $\langle x \rangle$, $\langle y \rangle$, $\langle x^2 \rangle$ and $\langle y^2 \rangle$ for each ensemble, and demanded that $\langle x \rangle$ and $\langle y \rangle$ be close to zero and that $\langle x^2 \rangle$ and $\langle y^2 \rangle$ remain constant apart from statistical fluctuations. At low values of g ($\simeq 0.25$) we had to increase to $N_T = 2000$ to ensure this, which was achieved by taking the last path of a run as input for the next, at the same values of the parameters. We also did a "cooling run," starting at $g = 0.5$ and decreasing in steps of 0.05 to $g = 0.25$, by taking the last path of the run at g as input for the run at $g - 0.5$. For this cooling run we took $a = 0.5$.

In fig. 14 we compare our Monte Carlo results for (a): $\Delta E \equiv E^{-+} - E^{++}$, (b): E^{++} and (c): $\Delta E' = E^{+-} - E^{++}$ with Rayleigh-Ritz variational results. The energy difference $\Delta E = E^{-+} - E^{++}$ was measured with the time correlation $\langle x(0)x(t) \rangle \sim \mathrm{e}^{-\Delta E \cdot t}$. The ground-state energy E^{++} follows from the virial theorem [38,39] $E^{++} = \langle (2x^2 - 1)(x^2 - 1)y^2 \rangle$, and the energy difference $\Delta E' = E^{+-} - E^{++}$ was measured using the time correlation $\langle y(0)y(t) \rangle \sim \mathrm{e}^{-\Delta E' \cdot t}$. Since we expect systematic errors to be much larger than statistical errors, fig. 14 displays the range of values obtained by varying a, N and N_T within the above-mentioned bounds. At lower g values, thermalisation problems are clearly visible in the energy differences, whereas for the ground-state energy, finite-a corrections will dominate. The discussion of Shuryak and Zhirov [39] on these errors is appropriate.

Figs. 15 and 16 give the scatter plots for $g = 0.25$ and $g = 0.5$ ($a = 0.5$, $N = 10\,000$, and $N_T = 2000$ and 500 respectively). One can clearly see the onset of tunneling.

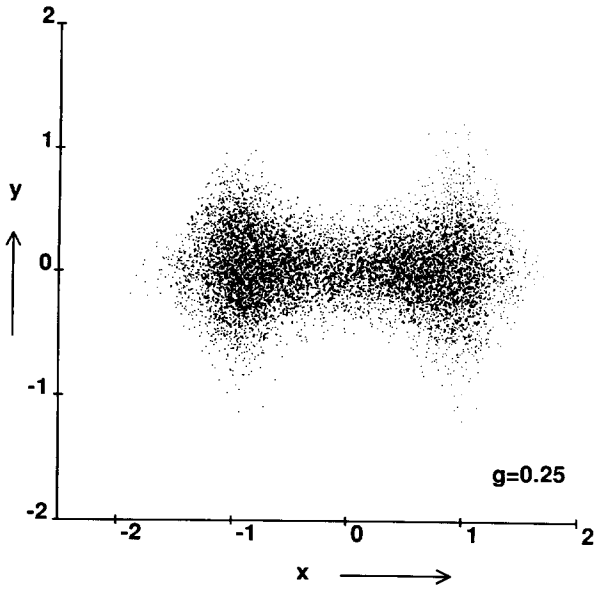

Fig. 15. Scatter plot for the toy-model at $g = 0.25$. We took the last path based on $N = 10\,000$, i.e. $(X(t_i), Y(t_i))$ for $i = 1$ to 10 000.

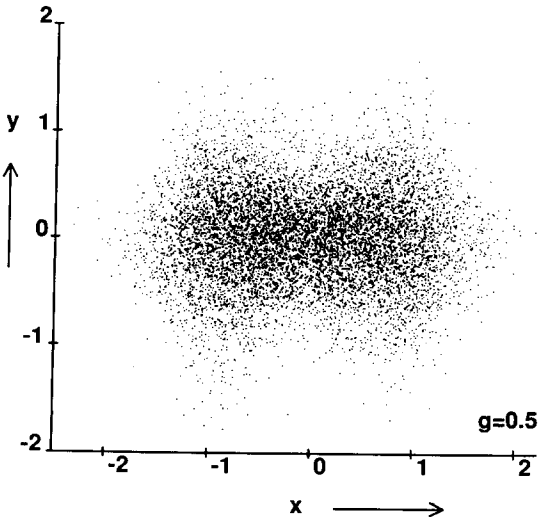

Fig. 16. Scatter plot for the toy-model at $g = 0.5$. We took the last path based on $N = 10\,000$, i.e. $(X(t_i), Y(t_i))$ for $i = 1$ to 10 000.

Appendix C

In this appendix we show how to obtain analytic expressions for the plane-wave radial matrix elements

$$F_e(n, n', l, i, j) = \int_0^\pi \mathrm{d}r\, r^{2+2i+2j} j_l\left(k_{n,l}^{(e)} r\right) j_{l+2j}\left(k_{n',l+2j}^{(e)} r\right). \tag{C.1}$$

The momenta $k_{n,l}^{(e)}$ depend on the electric flux (e), and are essentially roots of either the spherical Bessel function j_l or of its derivative:

$$j_l\left(\pi k_{n,l}^{(1)}\right) = 0,$$

$$\left.\frac{\mathrm{d}}{\mathrm{d}z}\left(z j_{n,l}(z)\right)\right|_{z=\pi k_{n,l}^{(0)}} = 0. \tag{C.2}$$

We first simplify by defining

$$f(w, z, l, p, q) = \int_0^1 \mathrm{d}y\, y^{2(1+p+q)} j_l(wy)\, j_{l+2q}(zy), \tag{C.3}$$

so that

$$F_l(n, n', l, p, q) = \pi^{3+2p+2q} f\left(\pi k_{n,l}^{(e)}, \pi k_{n',l+2q}^{(e)}, l, p, q\right). \tag{C.4}$$

The integral in eq. (C.3) can be calculated analytically for arbitrary w and z. The method is iterative, and we will briefly outline the algorithm.

For $p = q = 0$, l any integer, the integral is known [19], being given by the Lommel formula

$$\int_0^1 \mathrm{d}y\, y^2 j_l(zy)\, j_l(wy) = \frac{j_l(z)(w j_l(w))' - j_l(w)(z j_l(z))'}{z^2 - w^2}. \tag{C.5}$$

Using the recursion relations for spherical Bessel functions, one can derive the following recursion formulae for f:

$$f(w, z, l+1, p+1, 0) = (zw)^l \frac{\mathrm{d}^2}{\mathrm{d}w\,\mathrm{d}z} (zw)^{-1} f(w, z, l, p, 0), \tag{C.6a}$$

$$f(w, z, l, p, q+1) = z^{l+2q+1} \frac{\mathrm{d}}{\mathrm{d}z}\left(\frac{1}{z}\frac{\mathrm{d}}{\mathrm{d}z}\left[z^{-(l+2q)} f(w, z, l, p, q)\right]\right). \tag{C.6b}$$

In principle, eqs. (C.5), (C.6a) and (C.6b) determine the integrals, but they can be turned into a more convenient form as follows. Note that (although it is not

obvious) the ansatz

$$f(w, z, l, p, q) = A_{11} \cdot j_l(w)\, j_{l+2q}(z) + A_{12} \cdot j_l(w)\big(z j_{l+2q}(z)\big)' + A_{21} \cdot \big(w j_l(w)\big)' j_{l+2q}(z) + A_{22} \cdot \big(w j_l(w)\big)' \big(z j_{l+2q}(z)\big)', \quad \text{(C.7)}$$

is preserved under (C.6), with A_{mn} rational in w, z, l, p, q. Thus we obtain recursion relations for the rational functions, which can be iterated using an algebraic manipulation programme.

To obtain matrix elements, one has to substitute the relevant values for w and z, which further simplifies the result, since all except one of the terms in (C.7) then vanishes. However, a complication is that the coefficients A_{mn} involve $1/(z^2 - w^2)$, so that to set $w = z$ for the diagonal elements one first has to expand to some reasonably high order in $(w - z)$ and let the pole terms cancel (which they do). A further simplification is that when one normalises the wave functions, even the factors of j_l and its derivative drop out of the final answer, so the radial matrix elements are rational functions of the $k_{ln}^{(e)}$.

We are grateful to J. Vermaseren, who developed a very quick computer algorithm, that enabled us to confirm our results independently. Of course, one can also evaluate (C.3) numerically as a check, which we have done.

We do not discuss radial matrix elements in the harmonic oscillator case, since in the case with a boundary at π we had to resort to numerical integration, whereas with the boundary at infinity, we believe the simple results must be well known.

References

[1] G. 't Hooft, Nucl. Phys. B153 (1979) 141
[2] G. 't Hooft and M. Veltman, Nucl. Phys. B44 (1972) 189;
G. 't Hooft, Nucl. Phys. B61 (1973) 455;
M. Lüscher, Ann. Phys. (NY) 142 (1982) 359
[3] M. Lüscher, Nucl. Phys. B219 (1983) 233;
M. Lüscher and G. Münster, Nucl. Phys. B232 (1984) 445
[4] P. van Baal and J. Koller, Ann. Phys. (NY) 174 (1987) 299
[5] J. Koller and P. van Baal, Nucl. Phys. B273 (1986) 387
[6] J. Koller and P. van Baal, Phys. Rev. Lett. 58 (1987) 2511
[7] P. van Baal and A. Auerbach, Nucl. Phys. B275 [FS17] (1986) 93
[8] P. van Baal, Nucl. Phys. B264 (1986) 548
[9] T.H. Hansson, P. van Baal and I. Zahed, Nucl. Phys. B289 (1987) 628
[10] I. Zucker, J. Phys. A8 (1975) 1734
[11] V. Gribov, Nucl. Phys. B139 (1978) 1
[12] I. Singer, Comm. Math. Phys. 60 (1978) 7
[13] T. Killingback, Phys. Lett. 138B (1984) 87
[14] W. Nahm, *in* IV Warsaw Symp. on Elem. Part. Phys., ed. Z. Ajduk (Warsaw, 1981) p. 275
[15] R. Jackiw, I. Muzinich and C. Rebbi, Phys. Rev. D17 (1978) 1576
[16] N.M. Christ and T.D. Lee, Phys. Rev. D22 (1980) 939
[17] P. van Baal and J. Koller, Phys. Rev. Lett. 57 (1986) 2783

[18] M. Reed and B. Simon, Methods of modern mathematical physics, vol. 4 (Academic Press, New York, 1972)
[19] M. Abramowitz and I. Stegun, Handbook of mathematical functions (Dover, New York, 1978)
[20] B. Berg, A. Billoire and C. Vohwinkel, Phys. Rev. Lett. 57 (1986) 400
[21] B. Berg and A. Billoire, Nucl. Phys. B221 (1983) 109
[22] I.J. Muzinich and V.P. Nair, Phys. Lett. 178B (1986) 105
[23] R.D. Pisarski and O. Alvarez, Phys. Rev. D26 (1982) 3735;
J.F. Arvis, Phys. Lett. 127B (1983) 106;
P. Olesen, Phys. Lett. 160B (1985) 144, 408
[24] J. Kuti, *in* Proc. of Lattice gauge theory 1986, ed. H. Satz (Plenum, New York, 1987)
[25] P. van Baal, *in* Proc. of Lattice gauge theory 1986, ed. H. Satz (Plenum, New York, 1987)
[26] G. 't Hooft, Acta Phys. Austriaca, Suppl. 22 (1980) 531;
G. 't Hooft, Nucl. Phys. B190 [FS3] (1981) 955
[27a] B. Berg and A. Billoire, Phys. Lett. 166B (1986) 203; 185B (1987) 466E
[27b] G. Mack and E. Pietarinen, Phys. Lett. 94B (1980) 397
[28] B. Berg, *in* Proc. of Lattice gauge theory 1986, ed. H. Satz (Plenum, New York, 1987)
[29] M. Teper, Phys. Lett. 171B (1986) 81, 86;
J. Hoek, M. Teper and J. Waterhouse, Nucl. Phys. B288 (1987) 589
[30] Y. Arian and P. Woit, Phys. Lett. 169B (1986) 402;
I.A. Fox, J.P. Gilchrist, M.L. Laursen, and G. Schierholz, Phys. Rev. Lett. 54 (1985) 749
[31] J. Greensite and M.B. Halpern, Nucl. Phys. B271 (1986) 379
[31] P. Olesen, Phys. Scripta 23 (1981) 1000
[33] G. 't Hooft, Nucl. Phys. B138 (1978) 1
[34] M. Lüscher, Comm. Math. Phys. 104 (1986) 177; 105 (1986) 153
[35] M. Lüscher, Phys. Lett. 118B (1982) 391
[36] O.V. Tarasov, A.A. Vladimirov and A. Yu. Zharkov, Phys. Lett. 93B (1980) 429
[37] T.A. DeGrand, Colorado preprint COLO-HEP-138 (December 1986)
[38] M. Creutz and B. Freedman, Ann. Phys. 132 (1981) 427
[39] E.V. Shuryak and O.V. Zhirov, Nucl. Phys. B242 (1984) 393